bioRxiv preprint doi: https://doi.org/10.1101/514943; this version posted January 9, 2019. The copyright holder for this preprint (which was not certified by peer review) is the author/funder, who has granted bioRxiv a license to display the preprint in perpetuity. It is made available under aCC-BY-ND 4.0 International license.

Mycobacterium tuberculosis hijacks an evolutionary recent IFN-IL-6-CEBP axis linked to monocyte development and disease severity in humans

Murilo Delgobo[a], Edgar Kozlova[a], Edroaldo Lummertz Rocha[a,b], Gabriela F. Rodrigues-Luiz[a], Daniel A. G. B. Mendes[a], Lucas Mascarin[a], Greicy Dias[a], Daniel O. Patricio[a], Tim Dierckx[c], Maíra A. Bicca[a], Gaëlle Breton[d], Darcita Rovaris[e], Joanita Del Moral[f], Daniel S. Mansur[a], Johan Van Weyenbergh[c] and André Báfica[a,1]

[a]Laboratório de Imunobiologia, Departmento de Microbiologia, Imunologia e Parasitologia, Universidade Federal de Santa Catarina, Florianópolis, SC, 88040-900, Brazil
[b]Boston Children's Hospital Boston, MA
[c]Department of Microbiology and Immunology, Rega Institute for Medical Research, Laboratory for Clinical and Epidemiological Virology, KU Leuven - University of Leuven, Leuven, Belgium
[d]Laboratory of Molecular Immunology, The Rockefeller University, New York, NY 10065
[e]Laboratório Central do Estado de Santa Catarina/LACEN, Florianópolis, SC, 88040-900, Brazil
[f]Serviço de Hematologia, Hospital Universitário, Universidade Federal de Santa Catarina

[1]Lead contact
*Correspondence
andre.bafica@ufsc.br (A.B.)
johan.vanweyenbergh@kuleuven.be (J.V.W.)

Running title
M. tuberculosis hijacks IL-6R-mediated monocyte expansion in humans.

Authors' contribution:
MD, EK, ELR, GL, TD, DSM, JVW and AB designed experiments and analyzed data; MD, EK, JVW, DGM, LM, GD, DP, EK, GL, TD, MAB, ELR and AB performed experiments; GB, DR, JDM contributed with critical reagents/tools/clinical samples; AB, MD and JVW wrote the manuscript.

bioRxiv preprint doi: https://doi.org/10.1101/514943; this version posted January 9, 2019. The copyright holder for this preprint (which was not certified by peer review) is the author/funder, who has granted bioRxiv a license to display the preprint in perpetuity. It is made available under aCC-BY-ND 4.0 International license.

Abstract

Following pathogen-induced injury, multicellular organisms enhance production and differentiation of leukocytes, which are important players maintaining the body homeostasis. Monocyte counts are increased during human tuberculosis but it has not been determined whether *Mycobacterium tuberculosis* (*Mtb*) can regulate myeloid commitment. We demonstrated that following exposure to laboratory or clinical *Mtb* strains, primary $CD34^+$ cells preferentially differentiated into monocytes/macrophages, and to lesser extent granulocytes. This process required pathogen viability and while *Mtb* induced type I IFN expression and STAT1 phosphorylation in $CD34^+$ cells, myeloid conversion did not require type I or type II IFN signaling. In contrast, *Mtb* enhanced IL-6 production by $CD34^+$ cell cultures and IL-6R blockade abolished myeloid differentiation and decreased mycobacterial growth. Integrated systems biology analysis of transcriptomic, proteomic and genomic data of > 1,500 individuals from cohorts of healthy controls, latent and active tuberculosis (TB) patients confirmed the existence of a myeloid IL-6/IL-6R/CEBP axis associated with disease severity in vivo. Furthermore, genetic and functional analysis revealed the *IL6/IL6R/CEBP* gene module has undergone recent evolutionary selection, including Neandertal introgression, linked to systemic monocyte counts. Together, these results suggest *Mtb* hijacks an evolutionary recent IFN-IL6-CEBP feed-forward loop, increasing myeloid differentiation linked to severe TB in humans.

bioRxiv preprint doi: https://doi.org/10.1101/514943; this version posted January 9, 2019. The copyright holder for this preprint (which was not certified by peer review) is the author/funder, who has granted bioRxiv a license to display the preprint in perpetuity. It is made available under aCC-BY-ND 4.0 International license.

Hematopoiesis, the development of different blood cell lineages from hematopoietic stem cells (HSCs), is a fundamental physiological process in vertebrates. HSCs give rise to lineage-restricted progenitors that gradually differentiate into mature cells. Following cellular differentiation, single-lineage elements including erythrocytes, megakaryocytes, lymphocytes as well as myeloid cells such as monocytes and granulocytes circulate throughout the body performing diverse functions. While HSC development towards cellular lineages during homeostasis has been extensively studied[1], the mechanisms by which how progenitors give rise to mature cells during stress responses are less comprehended. For instance, certain pathogens regulate production of blood cells by the bone marrow and it has been shown that fine-tuned regulation of cytokine-induced signals is required for differentiation of HSC into mature cell types[2-4]. For example, the protozoan parasite that causes kalazar, *Leishmania donovani,* inhabits the bone marrow of humans[5] and induces differentiation of myeloid cells at expense of lymphoid progenitors[6]. In the same line of evidence, after experimental exposure to Gram-negative bacteria, mice display increased amounts of bone marrow-derived neutrophils, through a G-CSF–C/EBPα dependent mechanism[7]. Moreover, infection by intracellular bacteria has been shown to stimulate production of circulating monocytes[8-9]. Altogether, these studies indicate vertebrate hosts respond to infection by focusing specialized cell lineages, which are highly dependent upon the interplay of cytokine-induced hematopoiesis triggered during infection. Interestingly, recent reports have demonstrated stem/progenitor cells may be infected by different classes of infectious agents such as virus[10] and bacteria[11], albeit at low efficiency[11]. Therefore, since many pathogens may reach the bone marrow and provide microbial-HSC interactions, it is possible that, in addition to cytokines, pathogen recognition by progenitor stem cells directly regulate cell lineage commitment providing an anti-microbial defense system. In contrast, the Red Queen hypothesis[12] predicts such

bioRxiv preprint doi: https://doi.org/10.1101/514943; this version posted January 9, 2019. The copyright holder for this preprint (which was not certified by peer review) is the author/funder, who has granted bioRxiv a license to display the preprint in perpetuity. It is made available under aCC-BY-ND 4.0 International license.

pathogens would benefit from cell lineage commitment to establish themselves into the host.

The human pathogen *Mycobacterium tuberculosis* (*Mtb*) has been recently detected in circulating hematopoietic stem cells (Lin^-CD34^+) from latent TB individuals[13]**.** Since *Mtb* can also gain access to the bone marrow during extra-pulmonary[14] as well as active pulmonary TB[15], it has been suggested that the human bone marrow is a niche/reservoir for this bacterium during active or latent infection. However, whether interactions between *Mtb* and human $CD34^+$ cells drive cellular differentiation has not been formally demonstrated. Interestingly, during active TB, myeloid cells have been shown to display alterations such as increased numbers in the periphery[16-17] and dysregulated interferon-induced transcriptional signature[18-19]. More specifically, several interferon-inducible genes are modulated in circulating mature neutrophils and monocytes, as opposed to lymphocytes, in active TB patients, which calls forth a possible role of these genes in TB pathogenesis[18-20]. In contrast, lymphocyte compartments were recently demonstrated to be contracted during progression from latent to active TB in humans[21]**.** Based on this evidence, we hypothesized that *Mtb* regulates cellular differentiation of $CD34^+$ hematopoietic cell progenitors during TB.

Results

1. *Mtb* H37Rv replicates in primary human HSPC cultures. To formally investigate the dynamics of *Mtb* infection by hematopoietic stem cell progenitors (HSPCs), we have exposed peripheral blood mononuclear cells (PBMCs) from healthy donors to H37Rv *Mtb* and employed different techniques to measure bacterial infectivity by $CD34^+$ cells. Following 4h exposure to mycobacteria (multiplicity of infection, MOI3), flow cytometry experiments confirmed fluorescent *Mtb* were associated with $CD34^+$ cells (Figs. 1a, b and Supplementary Fig. 1a). At that time point, we observed ~69% of $CD34^+$ and ~79%

bioRxiv preprint doi: https://doi.org/10.1101/514943; this version posted January 9, 2019. The copyright holder for this preprint (which was not certified by peer review) is the author/funder, who has granted bioRxiv a license to display the preprint in perpetuity. It is made available under aCC-BY-ND 4.0 International license.

of CD14$^+$ associated with *Mtb* (Fig 1c). However, numbers of bacteria/CD34$^+$ cell, by means of MFI measurements, were found to be significantly lower when compared to those seen in CD14$^+$ cells (Fig. 1d). These data suggested that while CD34$^+$ cells may be permissive to *Mtb* infection in vitro, only low numbers of bacteria were associated with these cells. This idea was supported by confocal microscopy analysis, which confirmed the presence of few intracellular mycobacteria in purified CD34$^+$ cells at 4h p.i. (Supplementary Fig. 1b). These results raised the possibility that although human primary CD34$^+$ cells can be infected by *Mtb* in vitro (Supplementary Fig. 1b) and in vivo[13], this cell population displayed intrinsic resistance to *Mtb* infection as it has been reported for other bacterial species[11]. However, when purified CD34$^+$ cells were exposed to *Mtb* H37Rv (MOI3) and cultivated in conditioned media[22,23], bacilli numbers exhibited a significant ~1.5-log growth at 5 days post infection (dpi) (Fig. 1e). Similarly, kinyoun staining procedure confirmed the increased number of bacteria over time in the same cell cultures (Fig. 1f). Together, these data demonstrated that *Mtb* infects and replicates in primary human CD34$^+$ cell cultures in vitro. While at 1 dpi bacilli were more associated with the surface of round cells (Fig. 1f), at 5 d.p.i. intracellular bacteria appeared to be present in cells with abundant cytoplasm (Fig. 1f), thus indicating that *Mtb*-exposed CD34$^+$ cells displayed significant morphological alterations. These results were confirmed by Giemsa staining (Fig. 1g, arrows) which showed increased frequency of cytoplasm richer cells and indicated the possibility that *Mtb* enhances cellular differentiation in CD34$^+$ cells.

2. Live Mtb induces HSPCs towards myeloid differentiation and monocyte output.

To further explore whether *Mtb* triggered cellular differentiation by human purified CD34$^+$ cells in vitro, we first performed RNA-seq analysis of *Mtb*-exposed cells at different days post-infection and evaluated differential expression of 180 transcription factors (TFs)

bioRxiv preprint doi: https://doi.org/10.1101/514943; this version posted January 9, 2019. The copyright holder for this preprint (which was not certified by peer review) is the author/funder, who has granted bioRxiv a license to display the preprint in perpetuity. It is made available under aCC-BY-ND 4.0 International license.

previously described to be associated with differentiation of distinct hematopoietic cells[24] (Supplementary Fig. 1c). Interestingly, *Mtb* infection increased the expression of lineage-specific regulators of myeloid (GRAN/MONO) (*SPI1, CEBPB, CEBPA, EGR2 and STAT2*), but not lymphoid (B and T CELL) (*GABPA, SOX5, TCF3, GATA3, LEF1, RORA and LMO7*) or megakaryoid/erythroid (EARLY/LATE ERY) (*GATA1, FOXO3, NFE2, TAL1*) differentiation (Fig. 2a). Similarly, CellRouter signature score of the GRAN/MONO gene set was found to be increased in *Mtb* vs uninfected samples in all time points studied (Fig. 2b). Next, we applied a recently developed network biology-built computational platform[25] which, based on classification scores, can assess the extent to which a given population resembles mature cell types. Figure 2c shows that mRNA samples from *Mtb*-exposed $CD34^+$ cells presented enrichment of monocyte/macrophage profiles, but not other mature cell populations such as lymphocytes or dendritic cells. Additionally, at day 5 post-*Mtb* infection, $CD34^+$ cell cultures from 5 different donors displayed increased frequencies of CD11b (Fig. 2d), a surface molecule expressed during myeloid differentiation[26,27]**.** Together, these data suggested that *Mtb* drives human primary $CD34^+$ cells towards myeloid differentiation. To further approach this hypothesis, we employed multiparametric flow cytometry by measuring expression of cell surface molecules functionally associated with myeloid differentiation of human $CD34^+$ cells[28-31]. More specifically, we gated on $CD34^+$ events and evaluated %$CD64^+$ cells, since it has been demonstrated that human $CD64^+CD34^+$ progenitors generate monocytes and granulocytes[30-32]. Additionally, we included CD4 in the gating strategy as a second cell surface marker of human myeloid differentiation as previously demonstrated [32]. Corroborating our hypothesis, *Mtb* enhanced the frequency of $CD64^+CD4^+CD34^+$ cells (Fig. 2d-f) at 5 d.p.i., but not $CD10^+CD34^+$ (lymphoid) or $CD41a^+CD34^+$ (megakaryoid) progenitors (Supplementary Fig. 2a). Similarly, Lin^-CD34^+ cells from human bone marrow or PBMC (Supplementary Fig. 2b,c) exposed to *Mtb* displayed increased

bioRxiv preprint doi: https://doi.org/10.1101/514943; this version posted January 9, 2019. The copyright holder for this preprint (which was not certified by peer review) is the author/funder, who has granted bioRxiv a license to display the preprint in perpetuity. It is made available under aCC-BY-ND 4.0 International license.

frequency of $CD4^+CD64^+CD34^+$ cells. Moreover, these cells were also found to display augmented levels of CD38 and HLA-DR (Supplementary Fig. 2b,c), two molecules associated with advanced stage of cellular differentiation[28, 33-34]. In addition, frequencies of $CD4^+CD64^+$ within purified $CD34^+$ cells were found to be increased in cultures exposed to live but not heat-killed (HK) H37Rv *Mtb* (Fig. 2e-g). These results suggested that the observed cellular phenotype was mostly due to activities of live pathogen and only partially to mycobacterial PAMPs such as TLR2 (Ara-LAM) or TLR9 (*Mtb* gDNA)[35,36] agonists which induced CD38 and HLA-DR, but not CD4 and CD64 expression in $CD34^+$ cells (Supplementary Fig. 3a). Importantly, increased frequency of $CD4^+CD64^+CD34^+$ cells was also observed when cell cultures were exposed to a clinical isolate of *Mtb* (Fig. 2f,h), ruling out a possible genetic factor associated with the laboratory strain H37Rv[37]. Furthermore, $CD34^+$ cell death was not enhanced by *Mtb* infection as demonstrated by the use of a live-and-dead probe and lactate dehydrogenase (LDH) quantification in cell culture supernatants (Supplementary Fig. 3b,c). Together, these data indicate live *Mtb* directs primary human $CD34^+$ cells towards myeloid differentiation in vitro.

Three mature cell populations can be generated during the process of myeloid commitment: monocytes, granulocytes and myeloid-derived dendritic cells[29,31,38]**.** To investigate whether *Mtb* stimulated HPSC differentiation into mature myeloid populations, purified cord blood-derived $CD34^+$ cells were exposed to *Mtb* and 10d later, surface molecules were measured by flow cytometry. Live H37Rv (Fig. 3a,e) or clinical isolate (Supplementary Fig. 3d) *Mtb* enhanced expression of the monocyte surface molecule CD14, confirming the observed monocyte output enrichment by *CellNet* analysis (Fig. 2c). Compared to control cell cultures, $CD14^+$ cells induced by *Mtb* displayed similar MFI expression of CD11b, HLA-DR, CD64 and CD16 (Fig. 3i). However, when compared to uninfected cultures, some but not all donors presented increased frequency of $CD14^+CD16^+$ monocytes following exposure to *Mtb* (Fig. 3j).

bioRxiv preprint doi: https://doi.org/10.1101/514943; this version posted January 9, 2019. The copyright holder for this preprint (which was not certified by peer review) is the author/funder, who has granted bioRxiv a license to display the preprint in perpetuity. It is made available under aCC-BY-ND 4.0 International license.

Moreover, albeit not statistically significant, *Mtb* enhanced the frequency of $CD16^+CD66b^+$ neutrophils in the majority but not all samples tested (Fig. 3b,f). In contrast, heat killed *Mtb* did not stimulate monocyte or neutrophil output (Fig. 3e,f). As expected (Fig. 2a-c and Supplementary Fig. 2a), when compared to uninfected cell cultures, megakaryoid/platelet- (Fig. 3c,g), dendritic cell- (Fig. 3d,h) or erythroid- (Supplementary Fig. 3e) associated markers showed no changes after exposure to *Mtb*. Altogether, these results suggest *Mtb* selectively favors generation of monocytes, and to lesser extent neutrophils, by $CD34^+$ cells in vitro.

3. *Mtb*-enhanced myeloid differentiation is mediated by IL-6R, but not type I or type II IFN signaling. Cytokines are important triggers of $CD34^+Lin^-$ differentiation in vivo and in vitro[39] and Reactome pathway analysis of genes differentially expressed between infected versus uninfected conditions displayed enrichment of "cytokine signaling in immune system" (Supplementary Fig. 1d; n=3 donors, 2 independent experiments). Among several genes, this pathway displayed a significant enrichment of *IL6* (Supplementary Table 1) and it was one of the factors present in the conditioned commercial cocktail media (SCF, TPO, IL-3, IL-6 and Flt3L) employed in our in vitro system. Moreover, cytokine receptors including *IL6R* (Fig. 4a) as well as their cytokine partners, containing *IL6* (Fig. 4b), were enriched in *Mtb*-exposed $CD34^+$cells. In addition, "interferon signaling" and "interferon alpha/beta" pathways were significantly enriched in *Mtb*-exposed $CD34^+$ cells (Supplementary Fig. 1d and Fig. 5a). Together, these data suggest *Mtb* enhances IL-6 and type I IFN signaling during myeloid differentiation in vitro and therefore, we decided to further investigate both pathways during this process. *Mtb*-exposed $CD34^+$ cell cultures displayed increased *IL6* expression by qPCR (Supplementary Fig. 4a) and, in some donors, *IFNA2*, *IFNB* and *IFNG* transcripts were also detected albeit at lower level relative to the former cytokine (Supplementary Fig.

bioRxiv preprint doi: https://doi.org/10.1101/514943; this version posted January 9, 2019. The copyright holder for this preprint (which was not certified by peer review) is the author/funder, who has granted bioRxiv a license to display the preprint in perpetuity. It is made available under aCC-BY-ND 4.0 International license.

4a). Interferon-stimulated genes (ISGs) such as *MX1*, *ISG15* and *IFI16* as well as IL-6R-stimulated genes such as *IL1RA*, *GRB2* and *CXCL8* were enhanced in *Mtb*-stimulated $CD34^+$ cells from 5 different donors (Supplementary Fig. 4b). In addition, IL-6 protein was found to be augmented in *Mtb*-infected cells when compared to uninfected cell cultures (Fig. 4c) and, in experiments with exogenous IL-6 added to $CD34^+$ cell cultures, this cytokine increased the frequency of $CD4^+CD64^+CD34^+$ cells (Supplementary Fig. 4c), confirming previous findings.[40] Altogether, these data pointed to IL-6 signaling as a possible pathway involved in *Mtb*-enhanced myeloid differentiation by $CD34^+$ cells. Therefore, we next investigated whether IL-6R signaling contributed to such phenotype. We utilized neutralizing monoclonal antibodies in our in vitro system and observed that neither type I nor type II IFN signaling pathways were required to *Mtb*-enhanced monocyte/granulocyte conversion (Figs. 4d,e and Supplementary Fig. 4d,e). Although conditioned commercial media induced IL-6R-dependent background levels (~5%) of $CD14^+$ monocytes and (~5%) $CD66b^+$ granulocytes (Fig. 4f-h), neutralizing anti-IL-6Ra antibody (α-IL-6R) abolished *Mtb*-enhanced myeloid differentiation seen in $CD34^+$ cell cultures (Fig. 4f-h). In contrast, megakaryoid, erythroid- or dendritic cell-associated surface molecules were unaltered in α-IL-6R-treated cell cultures (Supplementary Fig. 4f-h). Next, we asked whether IL-6R signaling was involved in pathogen growth observed during cellular differentiation. We observed that *Mtb*-exposed $CD34^+$ cultures treated with α-IL-6R (Fig. 4i) presented significantly lower CFU counts when compared with infected untreated control cell cultures, while α-IFNAR2 (Fig. 4j) or α-IFN-γ (Fig. 4k) did not affect CFU counts. These results suggest *Mtb* hijacks IL-6R-mediated myeloid differentiation by human $CD34^+$ cells in vitro.

bioRxiv preprint doi: https://doi.org/10.1101/514943; this version posted January 9, 2019. The copyright holder for this preprint (which was not certified by peer review) is the author/funder, who has granted bioRxiv a license to display the preprint in perpetuity. It is made available under aCC-BY-ND 4.0 International license.

4. The IL6/CEBP gene module is enriched in TB monocyte transcriptomes and correlates with systemic dissemination and disease severity. To investigate whether IL-6R signaling correlated with monocyte development and TB-associated pathology in vivo, we performed a comprehensive systems biology analysis integrating transcriptomic, proteomic and genomic data from published cohorts consisting of a total of >1500 healthy controls and patients with latent, active and disseminated TB[18,21,41-43] (Supplementary Table 2). First, we investigated whether monocytes from active TB display a potential *in vivo* IL-6/IL-6R signature by using Ingenuity Pathway analysis (IPA) to determine upstream regulators in $CD14^+$ monocyte transcriptomes[18]**.** As shown in Fig. 5a (upper panel), when compared to cells from healthy controls, *IL6, IL6ST, IL6R* and *STAT3* were significantly enriched in transcriptomes of purified monocytes isolated from active TB patients. As reported previously[18,43,44]**,** *STAT1* and *IL1B* were confirmed as significant upstream regulators in active TB monocytes (Fig. 5a upper panel). Strikingly, the two top upstream regulators in TB monocytes, *IRF1* and *STAT1*, were the only genes in common between the "Berry TB monocytes" (GSE19435, GSE19439, GSE19444), the "IL6/STAT3 pathway"
and the "in vivo IFN-β" signatures (both from Molecular Signatures Database[43]) (Fig. 5a lower panel), suggesting these genes might be regulated by both IL-6 and type I IFN during active TB in vivo. Since type I IFN and IL-6 share the ability to induce phosphorylation of both STAT1 and STAT3[45], we used GSEA to investigate if their downstream target genes could overlap. In addition to previously demonstrated type I IFN/STAT1[18], "IL6/STAT3 pathway" was significantly enriched in the whole blood TB disease signature (FDR-corrected $p<10^{-4}$, Supplementary Table 2). Interestingly, these pathways were also significantly enriched in a gene set recently linked to monocyte expansion in vivo, measured as monocyte:lymphocyte (ML) ratio[41] (Supplementary Table 2). In that study, Naranbhai et al.[41] demonstrated that genes associated with

bioRxiv preprint doi: https://doi.org/10.1101/514943; this version posted January 9, 2019. The copyright holder for this preprint (which was not certified by peer review) is the author/funder, who has granted bioRxiv a license to display the preprint in perpetuity. It is made available under aCC-BY-ND 4.0 International license.

increased ML ratio positively correlate with impaired control of mycobacterial growth in vitro, supporting a possible connection between monocyte expansion and *Mtb* survival. Additionally, increased IL-6/STAT3 protein levels and changes in $CD34^+$ and $CD38^+$ homeostasis were found to be early events in TB pathogenesis (Fig. 5b upper and lower panels), as suggested by our reanalysis of the plasma proteome upon disease progression from latent to active TB[21]. "IL6/STAT3 pathway"-associated proteins such as PLA2G2A, CRP, STAT3, IL-6 and CFB increased around 12 months before TB diagnosis (Fig. 5c,d), which was concomitant with significant changes in "IFN/IL6-shared" plasma markers (CXCL10, IFNAR1 and MMP9). Strikingly, these alterations preceded enrichment of the ML ratio gene set (6 months before diagnosis, $p<0.05$, Fig. 5d upper panel) and reduction of the CD34/CD38 gene markers, in agreement with our in vitro model of *Mtb*-enhanced $CD34^+$ differentiation ($CD34^+ \rightarrow CD34^+CD38^+ \rightarrow CD14^+$). Moreover, fold-changes were higher for "IL6/STAT3 pathway" genes than for "IFN/IL6-shared" genes, and significantly higher than "ML ratio" genes ($p<0.05$) or "CD34/myeloid differentiation" genes ($p<0.01$) (Fig. 5d lower panel). Reciprocally, IL-6-regulated transcriptomes also significantly overlap with both type I and II IFN signaling (Supplementary Table 2, $p=10^{-3}$-10^{-10}) and are enriched for stem cell/HSPC/$CD34^+$ gene sets (Supplementary Table 2, $p=10^{-4}$-10^{-10}). Together, these results suggested that IL-6/IL-6R signaling induces expression of ISGs as well as myeloid differentiation genes during active TB in humans. In support of this concept, TFs upstream of *Mtb*-enhanced ISGs such as pSTAT1, and myeloid differentiation such as CEBP family members (C/EBPα and C/EBPβ), were found to be upregulated in $CD34^+$ cells in vitro (Supplementary Fig. 4i). Furthermore, we observed that *CEBPs, IRF1* and *STAT1* as well as *STAT3 and ICSBP/IRF8* TFs were significantly enriched in infected $CD34^+$ transcriptomes (Fig. 5e and Supplementary Fig. 5a), which were associated with increased mycobacterial replication in vitro (Fig. 1e).

bioRxiv preprint doi: https://doi.org/10.1101/514943; this version posted January 9, 2019. The copyright holder for this preprint (which was not certified by peer review) is the author/funder, who has granted bioRxiv a license to display the preprint in perpetuity. It is made available under aCC-BY-ND 4.0 International license.

Tuberculosis pathogenesis is a convoluted process which interconnects mycobacterial dissemination, host inflammatory responses and systemic tissue pathology. Since IL-6R signaling enhanced myeloid differentiation (Fig. 4f-h) as well as *Mtb* growth in vitro (Fig. 4i) and the monocyte expansion (ML ratio) gene set was found to be enriched during TB progression in vivo (Fig. 5c lower panel), we reasoned that *Mtb* enhances IL-6/IL-6R signaling-mediated monocyte output, promoting immunopathology and TB disease. To further investigate this molecular link with disease severity in vivo, we examined large transcriptomic data sets of disseminated TB, which includes extrapulmonary and lymph node TB (GSE63548). The "IL6/STAT3 pathway" was found to be significantly enriched among differentially expressed genes in both extrapulmonary (FDR $p=10^{-3}$) and lymph node TB (FDR $p=10^{-4}$, Supplementary Table 2). Furthermore, downstream targets of *STAT3*, *CEBPB, CEBPD* (the genes encoding C-EBPβ/NF-IL6 and C-EBPδ/NF-IL6β) as well as other transcription factors driving myeloid/monocyte commitment (*SPI1*/*PU1 and ICSBP/IRF8*) (Supplementary Table 2) were significantly enriched in the *Mtb*-exposed $CD34^+$ cells, the Berry whole blood TB signature, the monocyte expansion (ML ratio) and the disseminated TB gene sets (Fig. 5f). On the other hand, ISRE (STAT1/STAT2) and IRF1, the major upstream regulators observed in TB monocyte transcriptome (Fig. 5a) and shared between IL-6 and IFN signaling (Fig. 5b), were enriched in the Berry whole blood TB signature, in the disseminated TB and in the *Mtb*-stimulated $CD34^+$ cells (Fig. 5f). In addition, we found significant enrichment of *CEBPB, SPI1/PU1* and *MEIS1*, but not *ISRE* targets in PBMC from active TB patients with BCG vaccine failure (Fig. 5f) suggesting that activation of specific pathways downstream of these TFs may overcome BCG-mediated protection in humans. Moreover, only *CEBPB* targets were significantly enriched in the monocyte expansion (ML ratio) gene set in healthy subjects (Fig. 5f), supporting its link with myeloid

bioRxiv preprint doi: https://doi.org/10.1101/514943; this version posted January 9, 2019. The copyright holder for this preprint (which was not certified by peer review) is the author/funder, who has granted bioRxiv a license to display the preprint in perpetuity. It is made available under aCC-BY-ND 4.0 International license.

differentiation during homeostasis. Interestingly, TF *MEIS1*, which has been demonstrated as a key player in pathogenic myeloid differentiation by leukemic cells[46,47], was highly enriched in disseminated TB transcriptomes (Fig. 5f). Since the *IL6/IL6R/STAT3/CEBP* axis was correlated with both systemic disease dissemination and monocyte expansion, two processes associated with TB disease[16,17], we next examined whether these genes might be connected to disease severity in a published cohort with detailed clinical parameters and transcriptome data[18]. As shown in Fig. 5g, *CEBPB* and *IL6R* transcript levels were strongly connected and significantly correlated with *STAT3* and inflammatory biomarkers such as C-reactive protein and erythrocyte sedimentation rate (not shown). In addition, *CEBPB* transcript levels were significantly higher in *Mtb*-positive vs. *Mtb*-negative sputum smears, and strongly correlated to tissue damage (Modal X-ray grade) and total symptom count, as well as systemic clinical parameters such as lymphocyte count, albumin and hemoglobin levels (Fig. 5g). Taken together, these results suggest the IL6/IL6R/STAT3/CEBP gene module is a major hub linked to monocyte expansion during *Mtb* infection in vivo and is amplified in severe pulmonary and extrapulmonary disease.

5. Recent genetic changes link IL6/IL6R/CEBP axis, monocyte expansion and TB pathogenesis in humans. The “type I IFN” signature found in active TB[18], shared with the IL-6-regulated gene set (this study), comprises a number of well-characterized ISGs with cross-species antiviral activity (IRF1, PKR/EIF2AK2, OAS and APOBEC family members), which have been undergoing strong purifying selection during primate evolution[48,49]. Moreover, recent studies have also suggested a primordial role for RNA viruses in driving recent human evolution, considering selective Neandertal introgression in a large number of antiviral effector molecules[50,51]. We thus investigated the IL6/IL6R/CEBP signaling pathway, its partial overlap with type I IFN signaling and its link

bioRxiv preprint doi: https://doi.org/10.1101/514943; this version posted January 9, 2019. The copyright holder for this preprint (which was not certified by peer review) is the author/funder, who has granted bioRxiv a license to display the preprint in perpetuity. It is made available under aCC-BY-ND 4.0 International license.

to monocyte expansion from an evolutionary perspective. We hypothesized that these gene modules maintained during successful antiviral hominid evolution are linked to monocyte expansion and human susceptibility to severe TB. As shown in Fig. 6a, both the "specific" IL6/C/EBPβ pathway (upper left panel) and the partially overlapping IL-6/IFN STAT1/STAT3 pathways (upper right panel, STRING protein-protein interaction $p<10^{-16}$ for both) displayed highly variable levels of conservation when compared to *Homo sapiens* (Fig. 6a lower panel). IL-6, IL-6R and C/EBP family members C/EBPα, C/EBPβ and C/EBPδ differ substantially throughout primate evolution and even among closely related hominids (*Pan troglodytes* and *Gorilla gorilla*), while both STAT1 and STAT3 remain largely conserved in most mammals, birds and reptiles (Fig. 6a lower panel). Upon analysis of cross-species type I IFN regulation from the 'mammalian interferome' database[18], we found that highly conserved mammalian ISGs significantly overlapped with the TB disease signature[18,20], as well as the IL6/STAT3 signaling pathway (Supplementary Table 2). As expected, the "IFN/IL6-shared" genes *CXCL10, CXCL9, STAT1, STAT2* displayed higher fold-changes upon type I IFN treatment across all 10 species (Fig. 6b). Interestingly, the "IL6/STAT3 pathway" genes *IL6, STAT3* and *SOCS3* were also significantly upregulated while *IL6R* was significantly down-regulated (Fig. 6b) when cells from 10 species were exposed to type I IFN. Among CD34/myeloid pathway genes, *ICSBP/IRF8* and *CD38* were strongly upregulated, but only in 4/10 and 2/10 species, respectively, while *ELF1* was homogenously and significantly upregulated in 9/10 species (Fig. 6b). These results suggest that type I IFN consistently regulates expression of IL-6 signaling and myeloid-associated genes in different species. However, among the entire *IL6/IL6R/CEBP/CD34* myeloid gene set, *CEBPB* was the top most variable ISG across mammalian evolution (CV >1000%, Fig. 6c). Remarkably, type I IFN-mediated transcriptional upregulation of both *CEBPB* and *CEBPD* (previously

bioRxiv preprint doi: https://doi.org/10.1101/514943; this version posted January 9, 2019. The copyright holder for this preprint (which was not certified by peer review) is the author/funder, who has granted bioRxiv a license to display the preprint in perpetuity. It is made available under aCC-BY-ND 4.0 International license.

identified as IL6-specific TFs, NF-IL6 and NF-IL6β, respectively) was absent in all mammals investigated and significant only in humans (Fig. 6c, inset). These results were validated in an independent, published data set[52], showing primate-specific (humans and macaques) upregulation of *CEBPB* and *CEBPD* (in contrast to rodents), upon stimulation with double-stranded RNA, one of the strongest type I IFN inducers (Supplementary Fig. 5b). Thus, transcriptional upregulation of C/EBP-β/C/EBP-δ by synergistic IL6- and type I IFN-signaling seems to be a relatively recent event in mammalian and primate evolution. In contrast, IFN-inducibility of both *IL6* and *STAT3* transcripts is conserved in most mammals, including humans (Fig. 6c, inset). Moreover, conserved mammalian ISGs[49] also significantly overlapped with the monocyte expansion (ML ratio) gene set (Supplementary Fig. 5c). While "IFN/IL6-shared" genes displayed larger effect sizes for ML ratio, as compared to "IL6-specific pathway" genes (Fig. 6d left panel), the opposite was observed for absolute monocyte counts (Fig. 6d lower right panel). These data recapitulate the IL6/IL6R-mediated effect on monocyte expansion we observed in $CD34^+$ cells in vitro (Fig. 4f-h). Hence, analysis of evolutionary pressure on the *IL6/CEBP/CD34* myeloid gene module reveals a "feed-forward" loop in the crosstalk between type I IFN and IL-6 signaling through *CEBPB* and *CEBPD*, which appeared to be recently acquired in mammalian evolution. The latter was confirmed by a significant enrichment of primate-selected genes in this pathway (Supplementary Table 2). Since genetic susceptibility and transcriptional response to intracellular pathogens has also shown significant links to Neandertal introgression, mainly in populations of European and Asian descent populations[50,53], we next explored enrichment for Neandertal introgression in the *IL6/IL6R/CEBPB/CD34* myelopoietic gene module. As shown in Figure 6e (Venn diagram), three genes with Neandertal introgression in the ML ratio gene set were significantly upregulated in *Mtb*-stimulated $CD34^+$ cells (*OAS1, OAS2,*

bioRxiv preprint doi: https://doi.org/10.1101/514943; this version posted January 9, 2019. The copyright holder for this preprint (which was not certified by peer review) is the author/funder, who has granted bioRxiv a license to display the preprint in perpetuity. It is made available under aCC-BY-ND 4.0 International license.

MT2A), while 7 genes shared between Neandertal and ML ratio gene sets were not differentially expressed in *Mtb*-exposed CD34^{+} cells (*DUSP16, FCGR2A, IFITM1, PPARGC1B, TNFSF13B, GRK5* and *CD8A*). *OAS1, OAS2* and *MT2A* transcripts had significantly higher effect sizes upon ML ratios, corresponding to monocyte expansion, as compared to other introgressed genes ($p<0.05$) and to all other genes shown to regulate ML ratio *in vivo* ($p<0.001$, Fig 6e right panel). Moreover, a recently identified introgressed Neandertal *trans* e-QTL (rs5743618)[50] has been associated to pediatric TB susceptibility in the Chinese Han population[54]. Biological pathway analysis of genes significantly regulated in *trans* of rs5743618 revealed IL-6/STAT3 signaling as significantly enriched (FDR $p=4.6x10^{-8}$) and *IL6* as the most connected gene (Supplementary Table 2 and Fig. 6f). Finally, when considering genome-wide human variation, three lines of evidence support our hypothesis of a pathogen-selected *IL6/IL6R/CEBP* gene module regulating monocyte expansion in vivo. First, several large GWAS studies (a total of >200,000 individuals from different ethnic backgrounds) have identified single-nucleotide polymorphisms (SNPs) in or adjacent to *IL6R, CEBPA-CEBPD-CEBPE* and *ICSBP/IRF8* genes (ranked in Fig. 6f and detailed in Supplementary Table 3) as significantly associated to blood monocyte counts. Second, gene-specific z-scores for human adaptation measured by Daub et al.[55] in 51 different populations worldwide have revealed polygenic adaptation to pathogens. All genes in our proposed *IL6/IL6R/CEBP* myeloid differentiation module (except *CXCL10*) had positive z-scores (Fig. 6f and Supplementary Table 3), indicating relatively higher levels of population differentiation, with the highest z-scores for *CEBPB*, *IL6* and *IL6ST*, respectively. In addition, IL6/STAT3 signaling (but not type I IFN signaling) was significantly enriched among the top 500 genes with extreme positive adaptation z-scores (Supplementary Table 3). Third, a strong genetic component significantly predicts

bioRxiv preprint doi: https://doi.org/10.1101/514943; this version posted January 9, 2019. The copyright holder for this preprint (which was not certified by peer review) is the author/funder, who has granted bioRxiv a license to display the preprint in perpetuity. It is made available under aCC-BY-ND 4.0 International license.

IL-6 production stimulated by *Mtb* in both human purified macrophages and PBMCs from a large cohort of healthy controls[56] with both GWAS and immunophenotyping (Supplementary Fig. 5d). More importantly, the genetic factor defined by Bakker et al.[56] as variance in cytokine production explained by genetics (corrected for age and gender) was significantly stronger for IL-6, as compared to IL-1β, IL-22 and IFN-γ, considering 10 different bacterial and viral stimuli (Supplementary Fig. 5d). As compiled in Fig. 6f, our multi-level analysis revealed significant genetic links shared between IL-6/IL-6R/CEBP signaling, $CD34^+$ myeloid differentiation, monocyte homeostasis and *Mtb* pathogenesis, which have undergone mammalian, primate and recent human selection, including Neandertal introgression and worldwide population-specific adaptation.

Discussion

Emerging evidence have suggested that *Mtb* establishes an infectious niche in the human bone marrow during active pulmonary TB[13]. This idea is corroborated by independent observations showing that human mesenchymal and hematopoietic stem cells were found to contain viable bacilli during *Mtb* infection[13,15]. Notably, elevated circulating monocyte and decreased lymphocyte numbers have been previously associated with active TB[16,17,41,57]. In the present study, we observed that *Mtb* hijacks and enhances IL-6R-mediated myeloid differentiation by human primary $CD34^+$ cells in vitro. The IL-6/IL-6R signaling-associated molecules such as C/EBPβ, C/EBPδ, STAT3 and their downstream targets were significantly enriched in cell transcriptomes from active TB patients. This pathway positively correlated with TB disease severity and systemic disease. Therefore, our data expands previous studies and raise a novel scenario in which *Mtb* skews myeloid development, mediated by IL-6 signaling, as a key step in TB pathogenesis.

bioRxiv preprint doi: https://doi.org/10.1101/514943; this version posted January 9, 2019. The copyright holder for this preprint (which was not certified by peer review) is the author/funder, who has granted bioRxiv a license to display the preprint in perpetuity. It is made available under aCC-BY-ND 4.0 International license.

While *Mtb* consistently enhanced IL-6 expression by purified CD34$^+$ cell cultures in all donors, type I IFN was detected in some but not all donors. However, ISGs were highly enriched in the *Mtb*-exposed samples suggesting that either low amounts of type I IFN were produced in infected cell cultures and/or IL-6 itself induces STAT1 activation by CD34$^+$ cells[58]**.** Furthermore, these results indicate *Mtb* is a potent stimulus to induce ISGs in primary human CD34$^+$ cells, similar to what has been reported for human macrophages[43]. Additionally, the "interferon inducible gene signature" induced by *Mtb* in circulating mature myeloid cells, which has been largely demonstrated to be associated with TB disease severity[18-20], was also seen in *Mtb*-exposed CD34$^+$ cell cultures in vitro (Supplementary Fig. 5e). However, while IL-6R signaling was involved in *Mtb* growth by CD34$^+$ cells under cellular differentiation, type I or type II IFN signaling was not. Although the ISG set was enriched in *Mtb*-exposed CD34$^+$ cells, our data suggest type I or type II IFN signaling do not mediate *Mtb*-induced monocyte development in vitro. Interestingly, in our previously characterized cohort of multiple sclerosis patients[59,60], IFN-β therapy in vivo did not significantly change monocyte or lymphocyte counts, nor did it increase the ML ratio after three months of treatment in patients with documented clinical response (Supplementary Fig. 5f), supporting the concept that type I IFN by itself is not sufficient to cause monocyte expansion in vivo.

It has not been determined how mature myeloid cell populations from active TB patients acquire the "ISG" signature. While monocytes and other cells may encounter *Mtb*-associated inflammatory stimuli in infected tissues (e.g.: lungs and liver), our data raises the possibility *Mtb* may activate these cells during their development in the bone marrow. We have not directly addressed whether circulating monocytes/granulocytes acquire their phenotype in the bone marrow, during development of myeloid progenitors in vivo. Nevertheless, a recent study by Norris and Ernst[61] demonstrated increased monocyte egress from the bone marrow in a murine model of *Mtb* infection. Considering

bioRxiv preprint doi: https://doi.org/10.1101/514943; this version posted January 9, 2019. The copyright holder for this preprint (which was not certified by peer review) is the author/funder, who has granted bioRxiv a license to display the preprint in perpetuity. It is made available under aCC-BY-ND 4.0 International license.

virulent *Mtb*[15] and attenuated mycobacteria (BCG) can easily access the bone marrow and stimulate IL-6[62-64] it is possible that individuals draining higher amounts of *Mtb* into the bone marrow display increased inflammatory alterations including IL-6R-mediated myelopoiesis, upregulation of IFN-stimulated responses and increased disease severity. Indeed, we found that enrichment of the IL6/IL6R/STAT3/CEBP axis positively correlated with systemic disease such as lymph node and extrapulmonary TB (Fig. 5f,g). In line with our observations, IL-6, C/EBPβ and SPI1/PU1 have been previously reported to be associated with TB susceptibility[65,66]. Moreover, several independent studies have also indicated a detrimental role of "IFN and IFN-induced genes" during *Mtb* infection in human TB[18,20,21,67,68] and murine models[69]**.** Our results expand these previous studies, revealing a link between the IL6/IL6R/CEBP gene module to monocyte development, mycobacterial dissemination and TB disease severity. Moreover, as evidenced from Scriba *et al*[41] and re-analyzed in the present study (Fig. 5d), both IFN and IL6 pathways are early events in TB pathogenesis, detectable in the plasma proteome >6 months before diagnosis. Nevertheless, a pivotal role for IL6/IL6R signaling has not been evident from previous "omics" approaches. While IL-6 signaling partly overlaps with type I IFN responses (Fig. 5a-c), mostly due to their shared ability to activate STAT1 and STAT3[46], whole blood transcriptomic analyses are predominated by an "IFN-inducible neutrophil signature"[18]. Therefore, the high numbers of neutrophils in the blood possibly mask differential expression of other gene sets in less frequent populations, such as monocytes, monocyte subsets and, in particular, $Lin^{-}CD34^{+}$ cells.

Interestingly, most ISGs present in the whole blood Berry TB signature[18], the Scriba et al. TB plasma proteome[41] and the Naranbhai et al. ML ratio gene set[41] displayed cross-species type I IFN-induction throughout mammalian evolution (Fig. 6b-d). In spite of a shared STAT1/STAT3 activation by type I IFN and IL-6, homeostatic

bioRxiv preprint doi: https://doi.org/10.1101/514943; this version posted January 9, 2019. The copyright holder for this preprint (which was not certified by peer review) is the author/funder, who has granted bioRxiv a license to display the preprint in perpetuity. It is made available under aCC-BY-ND 4.0 International license.

activation of CEBP-β is mostly IL-6-specific, as evidenced by data mining and STRING analysis (Fig. 6a), in keeping with its original description as NF-IL6[70]. Across species, *CEBPB* is the top most variable ISG of the entire IFN/IL6/CD34/myeloid gene set (Fig. 6c). However, in addition to conserved type I IFN-induced *IL6* and *STAT3* transcription in the species studied, IFN-inducibility of *CEBPB* and *CEBPD* mRNA appeared to be developed during hominid evolution. Our data support the concept that *Mtb* hijacks a feed-forward loop between IL-6/IL-6R/STAT3 and IFN/IFNAR/STAT1/IRF1, activating the C/EBP gene module during myeloid differentiation in vivo (Fig. 6g). Furthermore, this process is linked to monocyte expansion and disease severity. While this study points to an important role for human CEBPs in TB disease, further experiments will define the precise molecular mechanisms of each CEBP family member, specifically CEBP-β and CEBP-δ, during *Mtb* infection.

We postulate that IL-6R-mediated myeloid differentiation in the bone marrow is used by *Mtb* to establish an infection niche in the human host, contributing to disease severity and pathogen dissemination. Alternatively, since the lung may be a reservoir for hematopoietic progenitors[71], *Mtb* could also active extra-marrow myelopoiesis during natural infection. While these questions merit directly investigation, nonetheless, it has been shown that anti-IL-6R treatment does not increase immunopathology nor tissue *Mtb* H37Rv loads in Balb/c mice[72] corroborating a hypothetical use of IL-6R blockade in severe human TB[73]. In summary, our results reveal a recent evolutionary link between myeloid differentiation, TB severity and IL6-IL6-R/CEBP signaling, which represents a novel host-directed target for therapeutic intervention in a major human disease.

bioRxiv preprint doi: https://doi.org/10.1101/514943; this version posted January 9, 2019. The copyright holder for this preprint (which was not certified by peer review) is the author/funder, who has granted bioRxiv a license to display the preprint in perpetuity. It is made available under aCC-BY-ND 4.0 International license.

Acknowledgments

We thank Drs. José Henrique M. Oliveira/UFSC and João Trindade Marques/UFMG for their critical reading of this manuscript. This work was supported by Howard Hughes Medical Institute – Early Career Scientist (A.B.; 55007412), National Institutes of Health Global Research Initiative Program (TW008276; A.B.) and Comissão de Aperfeiçoamento de Pessoal de Nível Superior (CAPES) Computational Biology (D.S.M.; 23038.010048/2013-27), FWO (J.V.W.; G0D6817N) and VLAIO (T.D.). A.B. and D.S.M. are CNPq-PQ scholars.

Materials and Methods

Reagents. *Mtb* Ara-LAM was obtained from BEI Resources and used at 5 µg/mL. *Mtb* H37Rv genomic DNA was obtained from 28 days colonies growing in Löwenstein–Jensen medium by CTAB method as previously described[74]. Recombinant human (*rh)* IL-6 was purchased from Immunotools. Anti-IFNAR2A (clone MMHAR-2, PBL) and anti-IFN-γ (clone B27, Immunotools) neutralizing antibodies were used at 1 and 10 µg/mL, respectively and anti-IL-6R (Tocilizumab, Roche) was used at 1 µg/mL. Fluorescent dye Syto24 was obtained from Thermo Fisher Scientific.

Mycobacteria cultures. The virulent laboratory H37Rv *Mtb* strain and the clinical *Mtb* isolate (CS267) were maintained in safety containment facilities at LACEN and UFSC as described elsewhere[74]. Briefly, *Mtb* was cultured in Löwenstein-Jensen medium (Laborclin) and incubated for 4 weeks at 37ºC. Prior to use, bacterial suspensions were prepared by disruption in saline solution using sterile glass beads. Bacterial concentration was determined by a number 1 McFarland scale, corresponding to 3×10^8 bacteria/mL.

bioRxiv preprint doi: https://doi.org/10.1101/514943; this version posted January 9, 2019. The copyright holder for this preprint (which was not certified by peer review) is the author/funder, who has granted bioRxiv a license to display the preprint in perpetuity. It is made available under aCC-BY-ND 4.0 International license.

Subjects samples, cells and *Mtb* infections. This study was approved by the institutional review boards of Universidade Federal de Santa Catarina and The University Hospital Prof. Polydoro Ernani de São Thiago (IRB# 89894417.8.0000.0121). Informed consent was obtained from all subjects. Peripheral blood and bone marrow mononuclear cells were obtained using Ficoll-Paque (GE) in accordance with the manufacturer's instructions. Briefly, blood collected in lithium-heparin containing tubes was further diluted in saline solution 1:1 and added over one volume of Ficoll-Paque reagent. The gradient was centrifuged for 40 min at 400 x *g*, 20ºC. The top serum fraction was carefully removed, the mononuclear fraction was harvested and washed once in a final volume of 50 mL of saline solution for 10 min at 400 x *g*, 20ºC. Subsequently, cell pellet was suspended and washed twice with 20 mL of saline solution for 10 min at 200 x *g*, 20ºC, to remove platelets. Cells were then suspended to the desired concentration in RPMI 1640 (Life Technologies) supplemented with 1% fresh complement inactivated (30 min at 56ºC) autologous serum, 2 mM *L*-glutamine (Life Technologies), 1 mM sodium pyruvate (Life Technologies) and 25mM HEPES (Life Technologies). Human Cord Blood (CB) purified $CD34^+$ cells from 5 different donors were obtained from STEMCELL Technologies and resuspended in StemSpan Expantion Media – SFEM II (STEMCELL Technologies) according to manufacturer's instruction. Optimal cell density for replication was 5 x 10^4 $CD34^+$ cell/mL. Following 4 days of expansion, cells were washed and diluted in SFEM II media without cytokine cocktail to the desired concentration. Culture purity was assessed by FACS and showed more than 90% of $CD34^+$ events after expansion. For *in vitro* infection experiments, 1 McFarland scale was diluted in media to fit the desired multiplicity of infection (MOI). For each experiment, bacteria solution was plated in Middlebrook 7H10 agar (BD Biosciences) supplemented with 10% Oleic Acid Albumin Dextrose Complex (OADC) and incubated at 37ºC to confirm initial bacteria input. In a set of experiments, 1 McFarland scale was

bioRxiv preprint doi: https://doi.org/10.1101/514943; this version posted January 9, 2019. The copyright holder for this preprint (which was not certified by peer review) is the author/funder, who has granted bioRxiv a license to display the preprint in perpetuity. It is made available under aCC-BY-ND 4.0 International license.

incubated with 500 nM of Syto24 dye as described previously[74]. In some experiments, H37Rv *Mtb* was heat killed (HK) at 100°C for 30 min. In cytokine/cytokine neutralizing experiments, cells were pretreated with anti-IFNAR2 (1 µg/mL), anti-IFN-γ (10 µg/mL) or anti-IL-6R (1 µg/mL) for 1h and exposed to *Mtb* (MOI3). Following different time points post-infection, cells were harvest and centrifuged at 400 x *g* for 10 min, 20ºC. Supernatants were then stored at -20ºC, cells washed once in sterile saline solution and lysed by using 200 µL of 0.05% Tween 80 solution (Vetec) in sterile saline. Cell lysates were diluted in several concentrations (10^{-1} to 10^{-5}), plated onto Middlebrook 7H10 agar (BD Biosciences) supplemented with OADC 10% and incubated at 37ºC. After 28 days, colony-forming units (CFU) were counted and results were expressed graphically as CFU/mL.

Microscopy experiments. After different time points post-infection, cells were washed and fixed with PFA 2% overnight at 4ºC. Subsequently, cells were washed with sterile water solution and adhered into coverslips by cytospin centrifugation. Samples were then fixed with methanol for 5 min, washed with sterile water and stained with carbol-fuchsin (Sigma) for 2 min. Samples were washed once with sterile water and counterstaining was done with methylene blue dye (Sigma) for 30 sec. Coverslips were fixed in slides with Permount mounting medium (Sigma) and examined using Olympus BX40 microscope and digital camera Olympus DP72. Syto24-stained *Mtb* was visualized in $CD34^+$ cells by using confocal fluorescence-equipped inverted phase contrast microscope and photographed with a digital imaging system camera. Briefly, 1 x 10^5 $CD34^+$ cells were seeded in 24-well plate and infected with *Mtb* syto24, MOI3, for 4 h. Further, cells were washed, fixed with PFA 2% and adhered into coverslip by cytospin centrifugation. For nucleus visualization, cells were stained with Hoechst 33342 (Immunochemestry technologies) for 2h. Cells were after washed and mounted for analysis in Leica DMI6000 B confocal microscope.

bioRxiv preprint doi: https://doi.org/10.1101/514943; this version posted January 9, 2019. The copyright holder for this preprint (which was not certified by peer review) is the author/funder, who has granted bioRxiv a license to display the preprint in perpetuity. It is made available under aCC-BY-ND 4.0 International license.

Immunoblotting. $CD34^+$ cells were seeded at 3 x 10^5 cells in 24-well plate and infected with *Mtb* (MOI3). After 5 days of infection, cells were centrifuged at 4ºC, pellet was lysed using M-PER lysis buffer (Thermo Fisher Scientific) containing protease inhibitors (Complete, Mini Protease Inhibitor Tablets, Roche) and protein extracts were prepared according to manufacturer's instructions. For Western blot, 15 µg of total protein were separated and transferred to nitrocellulose difluoride 0.22 µm blotting membranes. Membranes were blocked for 1 h with TBST containing 5% w/v BSA and subsequently washed three times with TBST for 5 min each wash. Further, membranes were then probed with anti-pSTAT1 Y701 1:1000 (M135 – Abcam), anti-STAT1 1:1000 (SM1 – Abcam), anti-C/EBP β 1:250 (sc-150 – Santa Cruz) or anti-β-Actina 1:5000 (8226 – Abcam) primary antibodies diluted in 5% w/v BSA, 0.1% tween 20 in TBS, at 4ºC with gentle shaking overnight. Membranes were washed with TBST, incubated in secondary HRP-linked Ab for 2 h at room temperature, washed and chemiluminescence developed using ECL substrate (Pierce). Relative expression was normalized with β-actin control and pixel area was calculated using ImageJ software.

Flow cytometry. PBMC and bone marrow mononuclear cells were seeded at 5 x 10^5 cells per well in a final volume of 200 µL. After 4 h of resting at 37ºC with 5% CO_2, cells were infected with *Mtb* (MOI3) for 72h, unless indicated otherwise. Cells were detached from the plate by vigorous pipetting, centrifuged at 450 x *g* for 10 min and washed twice in saline solution and stained with fixable viability stain FVS V450 (BD Biosciences) at the concentration 1:1000 for 15 min at room temperature. Cells were then washed with FACS buffer (PBS supplemented with 1% BSA and 0.1% sodium azide) and incubated with 10% pooled AB human serum at 4ºC for 15 min. The following antibodies were used in different combinations for staining:

Staining of human $CD34^+$ in PBMC: anti-Lin1(CD3, CD14, CD16, CD19, CD20,CD56) (FITC, clones MφP9, NCAM 16, 3G8, SK7, L27, SJ25-C1), anti-CD34 (PE,

bioRxiv preprint doi: https://doi.org/10.1101/514943; this version posted January 9, 2019. The copyright holder for this preprint (which was not certified by peer review) is the author/funder, who has granted bioRxiv a license to display the preprint in perpetuity. It is made available under aCC-BY-ND 4.0 International license.

PE, clone 581), anti-CD34 (FITC, 8G12), anti-CD34 (PerCP, clone 581), anti-HLA-DR (PE-Cy7, clone L243), anti-HLA-DR (Bv510, clone G46-6), anti-CD38 (APC, clone HIT2), anti-CD4 (APC-Cy7,GK1.5), anti-CD64 (Bv421, clone 10.1), anti-CD10 (FITC, clone HI10A), anti-CD14 (V450, clone MoP9), anti-CD14 (Alexa488, clone M5E2) were added at titrated determined concentration and incubated for 40 min at 4ºC.

Staining of CB $CD34^+$ cells: anti-CD34 (PE, clone 581), anti-CD11b (clone), anti-CD4 (APC-Cy7, clone GK1.5), anti-CD64, (Bv421, MoP9), anti-CD14 (V450, clone MoP9) anti-CD14 (Alexa488, clone M5E2), anti-CD66b (PE, clone G10F5), anti-BDCA1 (APC-Cy7, clone L161), anti-CD41a (FITC, clone 6C9), anti-BDCA2 (APC, clone 201A), anti-BDCA3 (Bv510, clone 1A4), anti-Clec9A (A700, clone FAB6049P), anti-CD123 (PE, clone 7G3), anti-CD16 (APC, clone 3G8) were added at titrated determined concentrations and incubated for 40 min at 4ºC. All cells were subsequently washed with FACS buffer and resuspended in 2% PFA. Cells were acquired on BD FACS Verse with FACSuite software. Analysis were performed using FlowJo software v. 10.1 (TreeStar).

Real-time quantitative PCR. Total RNA was extracted from $CD34^+$ cells exposed or not with *Mtb*. RNA was extracted after 1, 3 and 5 days of infection using TRIzol reagent (Thermo) according to manufacturer's instruction. Using 1 µg of RNA, cDNA was produced with a High-Capacity cDNA Reverse Transcription Kit (Applied Biosystems) and 2 µL of 1:8 diluted product was used to the quantitative PCR reaction in a final volume of 10 µL. qPCR reactions were performed using the primers for: *IFNA2A* F: 5'-TTGACCTTTGCTTTACTGGT-3', R: 5'-CACAAGGGCTGTATTTCT TC-3'. *IL6* F: 5'-CCACACAGACAGCCACTCAC-3', R: 5'-AGGTTGTTTTCTGCCAGTGC-3'. *IFNG* F: 5'-TCAGCTCTGCATCGTTTTGG-3', R: 5'-GTTTCCATTATCCGCTACATCTGAA-3'. *IL1B* F: 5'-ACAGATGAAGTGCTCCTTCCA-3', R: 5'-GTCGGAGATTCGTAGCTGGAT-3'. *IFI16* F: 5'-ACTGAGTACAACAAAGCCATTTGA-3', R: 5'-TTGTGACATTGTCCTGTCCCCAC-3'. *MX1* F: 5'-ATCCTGGGATTTTGGGGCTT-3', R:

bioRxiv preprint doi: https://doi.org/10.1101/514943; this version posted January 9, 2019. The copyright holder for this preprint (which was not certified by peer review) is the author/funder, who has granted bioRxiv a license to display the preprint in perpetuity. It is made available under aCC-BY-ND 4.0 International license.

5'-CCGCTTGTCGCTGGTGTCG-3'. *ISG15* F: 5'-TCCTGGTGAGGAATAACAAGGG-3', R: 5'-CTCAGCCAGAACAGGTCGTC-3'. *CSF1* F: 5'-GGAGACCTCGTGCCAAATTA-3', R: 5'-TATCTCTGAAGCGCATGGTG-3'. *CSF2* F: 5'-CTCAGAAATGTTTGACCTCCAG-3', R: 5'-TGACAAGCAGAAAGTCCTTCAG -3'. *CXCL8* F: 5'-GAGGTGATTGAGGTGGACCAC-3', R: 5'-CACACCTCTGCACCCAGTTT-3'. *IL1RA* F: 5'-ATGGAGGGAAGATGTGCCTGTC-3', R: 5'-GTCCTGCTTTCTGTTCTCGCTC-3'. *GRB2* F: 5'-GAAATGCTTAGCAAACAGCGGCA-3', R: 5'-TCCACTTCGGAGCACCTTGAAG-3'.

RNA isolation and sequencing. Total RNA from CB $CD34^+$ cells exposed to *Mtb* in vitro and PBMCs from either healthy controls or patients with latent or active TB were isolated using TRIzol LS (Invitrogen; 10296010). RNAseq libraries were prepared using the Nugen Ovation Trio low input RNA Library Systems V2 (Nugen; 0507-08) according to the manufacturer's instructions by the Nucleomics Platform (VIB, Leuven, Belgium). Pooled libraries were sequenced as 150 bp, paired-end reads on an Illumina HiSeq 2500 using v4 chemistry.

RNAseq data quality assessment and differential expression analyses. Illumina sequencing adapters and reads with Phred quality scores lower than 20 were removed with Trimmomatic (0.36). Trimmed reads were aligned to *H. sapiens* reference genome (hg38) by STAR (2.6.0c). Aligned reads were mapped to genes using featureCounts from the Subread package (1.6.1). Genes with reads of less than 3 were removed. Library based normalization was used to transform raw counts to RPKM and further normalized using the edgeR TMM normalization (3.10.0). Data were then transformed using the limma voom function (3.36.2), prior to batch correction using ComBat (sva 3.28.0). Negative binomial and linear model-based methods were used for differential

bioRxiv preprint doi: https://doi.org/10.1101/514943; this version posted January 9, 2019. The copyright holder for this preprint (which was not certified by peer review) is the author/funder, who has granted bioRxiv a license to display the preprint in perpetuity. It is made available under aCC-BY-ND 4.0 International license.

expression analysis, using packages edgeR and limma packages. Differentially expressed genes (DEGs) were calculated with t-statistics, moderated F-statistic, and log-odds of differential expression by empirical Bayes moderation of the standard errors.

CellNet and CellRouter analysis. We applied CellNet to classify RNA-seq samples as previously described[25]. Raw RNA sequencing data files were used for CellNet analysis. The analysis pipeline is based on the R statistical programming language. We used R version 3.4.1, CellNet version 0.0.0.9000, Salmon[75] version 0.8.2 and the corresponding index downloaded from the CellNet website. We used CellRouter[76] to calculate signature scores for each sample based on cell-type specific transcriptional factors collected from literature. Specifically, for this analysis, we normalized raw counts by library size as implemented in the R package DESeq2[77]. We then plotted the distributions of signature scores across experimental conditions. Moreover, we used CellRouter to identify genes preferentially expressed in each experimental condition and used those genes for Reactome pathways enrichment analysis using the package Enrichr version 1.0.

Systems biology analysis. Ingenuity Pathway Analysis (IPA) software was used to perform the initial pathway/function level analysis on genes determined to be differentially expressed in transcriptomic analysis (Ingenuity Systems, Red Wood City, CA). Uncorrected p-values and absolute fold-changes were used with cut-offs of $p<0.05$ (monocyte transcriptomes from active TB patients) or $p<0.01$ (differentially expressed genes in *Mtb*-exposed $CD34^+$ cells and all publicly available datasets from GEO). Differentially expressed genes were sorted into gene networks and canonical pathways, and significantly overrepresented pathways and upstream regulators were identified. Additional pathway, GO (Gene Ontology) and transcription factor target enrichment analysis was performed using GSEA (Gene Set Enrichment Analysis, Broad Institute Molecular Signatures Database (MSigDB)) and WebGestalt (WEB-based GEne SeT AnaLysis Toolkit). Gene sets from GO, Hallmark, KEGG pathways, WikiPathways and

bioRxiv preprint doi: https://doi.org/10.1101/514943; this version posted January 9, 2019. The copyright holder for this preprint (which was not certified by peer review) is the author/funder, who has granted bioRxiv a license to display the preprint in perpetuity. It is made available under aCC-BY-ND 4.0 International license.

Pathway Commons databases, as well as transcription factor motifs, were considered overrepresented if their FDR-corrected p-value was smaller than 0.05. To validate our compiled IL6/IL6R/CEBP and $CD34^+$ myeloid differentiation gene modules, we used STRING (version 10.5) protein-protein interaction enrichment analysis (www.string-db.org), using the whole human genome as background. Principal component analysis, correlation matrices, unsupervised hierarchical (Eucledian distance) and k-means clustering were performed using XLSTAT and visualized using MORPHEUS (https://software.broadinstitute.org/morpheus/).

Data processing and statistical analyses. Data derived from in vitro experiments was processed using GraphPad Prism 6 software and analyzed using unpaired *t* test, one-way ANOVA or two-way ANOVA according to the experimental settings. Data from experiments performed in triplicate are expressed as mean ± SEM. Non-parametric tests (Mann-Whitney, Spearman correlation) were used for clinical data (sputum bacillar load, modal X-ray grade, symptom count) and molecular data that were not normally distributed, Pearson correlation was used for molecular data with a normal distribution. Statistical significance was expressed as follows: $*p \leq 0.05$, $**p \leq 0.01$ and $***p \leq 0.001$.

References

1 - Hoggatt, J., Kfoury, Y. & Scadden, D. T. Hematopoietic Stem Cell Niche in Health and Disease. *Annual Review of Pathology: Mechanisms of Disease* **11**, 555–581 (2016).

2 - Zhang, C. C. & Lodish, H. F. Cytokines regulating hematopoietic stem cell function. *Current Opinion in Hematology* **15**, 307–311 (2008).

3 - Mirantes, C., Passegué, E. & Pietras, E. M. Pro-inflammatory cytokines: Emerging players regulating HSC function in normal and diseased hematopoiesis. *Experimental Cell Research* **329**, 248–254 (2014).

4 - Kleppe, M. et al. Jak1 Integrates Cytokine Sensing to Regulate Hematopoietic Stem Cell Function and Stress Hematopoiesis. *Cell Stem Cell* **21**, 489–501.e7 (2017).

5 - Kumar, R. & Nylén, S. Immunobiology of visceral leishmaniasis. *Frontiers in Immunology* **3**, (2012).

bioRxiv preprint doi: https://doi.org/10.1101/514943; this version posted January 9, 2019. The copyright holder for this preprint (which was not certified by peer review) is the author/funder, who has granted bioRxiv a license to display the preprint in perpetuity. It is made available under aCC-BY-ND 4.0 International license.

6 - Abidin, B. M., Hammami, A., Stäger, S. & Heinonen, K. M. Infection-adapted emergency hematopoiesis promotes visceral leishmaniasis. *PLOS Pathogens* **13**, e1006422 (2017).

7 - Boettcher, S. et al. Endothelial cells translate pathogen signals into G-CSF-driven emergency granulopoiesis. *Blood* **124**, 1393–1403 (2014).

8 - MacNamara, K. C. et al. Infection-Induced Myelopoiesis during Intracellular Bacterial Infection Is Critically Dependent upon IFN-γ Signaling. *The Journal of Immunology* **186**, 1032–1043 (2010).

9 - Baldridge, M. T., King, K. Y., Boles, N. C., Weksberg, D. C. & Goodell, M. A. Quiescent haematopoietic stem cells are activated by IFN-γ in response to chronic infection. *Nature* **465**, 793–797 (2010).

10 - Carter, C. C. et al. HIV-1 Utilizes the CXCR4 Chemokine Receptor to Infect Multipotent Hematopoietic Stem and Progenitor Cells. *Cell Host & Microbe* **9**, 223–234 (2011).

11 - Kolb-Maurer, A. Interaction of human hematopoietic stem cells with bacterial pathogens. *Blood* **100**, 3703–3709 (2002).

12 – Van Valen, L. A New Evolutionary Law. *Evolutionary Theory*, **1**, 1-30 (1973).

13 - Tornack, J. et al. Human and Mouse Hematopoietic Stem Cells Are a Depot for Dormant Mycobacterium tuberculosis. *PLOS ONE* **12**, e0169119 (2017).

14 - Mert, A. et al. Miliary tuberculosis: Clinical manifestations, diagnosis and outcome in 38 adults. *Respirology* **6**: 217–224 (2001).

15 - Das, B. et al. CD271+ Bone Marrow Mesenchymal Stem Cells May Provide a Niche for Dormant Mycobacterium tuberculosis*. Science Translational Medicine* **5**, 170ra13-170ra13 (2013).

16 - Schmitt E., Meuret G. & Stix L. Monocyte recruitment in tuberculosis and sarcoidosis. *British Journal of Hematology* **35**(1): 11-7. (1977).

17 - Rogers PM: A study of the blood monocytes in children with tuberculosis. *New England Journal of Medicine* **198**: 740-749. (1928).

18 - Berry, M. P. R. et al. An interferon-inducible neutrophil-driven blood transcriptional signature in human tuberculosis. *Nature* **466**, 973–977 (2010).

19 - Zak, D. E. et al. A blood RNA signature for tuberculosis disease risk: a prospective cohort study. *The Lancet* **387**, 2312–2322 (2016).

20 - dos Santos, P. F. et al. ISG15-Induced IL-10 Is a Novel Anti-Inflammatory Myeloid Axis Disrupted during Active Tuberculosis. *The Journal of Immunology* **200**, 1434–1442 (2018).

bioRxiv preprint doi: https://doi.org/10.1101/514943; this version posted January 9, 2019. The copyright holder for this preprint (which was not certified by peer review) is the author/funder, who has granted bioRxiv a license to display the preprint in perpetuity. It is made available under aCC-BY-ND 4.0 International license.

21 - Scriba, T. J. et al. Sequential inflammatory processes define human progression from M. tuberculosis infection to tuberculosis disease. *PLOS Pathogens* **13**, e1006687 (2017).

22 – Bodine D.M., Crosier P.S. & Clark S.C. Effects of hematopoietic growth factors on the survival of primitive stem cells in liquid suspension culture. *Blood* **15**; 78(4):914-20. (1991).

23– Keller J.R., Ortiz M. & Ruscetti F.W. Stell factor (c-kit ligand) promotes the survival of hematopoietic stem/progenitor cells in the absence of cell division. *Blood* **1**; 86(5):1757-64 (1995).

24 - Novershtern, N. et al. Densely Interconnected Transcriptional Circuits Control Cell States in Human Hematopoiesis. *Cell* **144**, 296–309 (2011)

25 - Cahan, P. et al. CellNet: Network Biology Applied to Stem Cell Engineering. *Cell* **158**, 903–915 (2014).

26 – Rosmarin A.G. et al. Differential expression of CD11b/CD18 (Mo1) and myeloperoxidase genes during myeloid differentiation. *Blood* **73**(1): 131-6. (1989).

27– Hickstein D.D., Back A.L. & Collins S.J. Regulation of expression of the CD11b and CD18 subunits of the neutrophil adherence receptor during human myeloid differentiation. *The Journal of Biological Chemistry* **264**, 21812-21817. (1989).

28 - Cimato, T. R., Furlage, R. L., Conway, A. & Wallace, P. K. Simultaneous measurement of human hematopoietic stem and progenitor cells in blood using multicolor flow cytometry. *Cytometry Part B*: *Clinical Cytometry* **90**, 415–423 (2016).

29 - Manz, M. G., Miyamoto, T., Akashi, K. & Weissman, I. L. Prospective isolation of human clonogenic common myeloid progenitors*. Proceedings of the National Academy of Sciences* **99**, 11872–11877 (2002).

30 - Olweus J., Lund-Johansen F., & Terstappen L.W. CD64/Fc gamma RI is a granulo-monocytic lineage marker on CD34+ hematopoietic progenitor cells. *Blood* **85**(9): 2402-13. (1995).

31 - Kawamura, S. et al. Identification of a Human Clonogenic Progenitor with Strict Monocyte Differentiation Potential: A Counterpart of Mouse cMoPs. Immunity 46, 835–848.e4 (2017).

32 - Gorczyca, W. et al. Immunophenotypic Pattern of Myeloid Populations by Flow Cytometry Analysis. *in Methods in Cell Biology* 221–266 (Elsevier, 2011).

33 - Terstappen L.W., Huang S., Safford M., Lansdorp P.M. & Loken M.R. Sequential generations of hematopoietic colonies derived from single nonlineage-committed CD34+CD38- progenitor cells. *Blood* **15**, 77(6): 1218-27. (1991).

34 - De Bruyn, et al. Comparison of the coexpression of cd38, cd33 and hla-dr antigens on cd34+ purified cells from human cord blood and bone marrow. *Stem Cells* **13**: 281–288. (1998).

bioRxiv preprint doi: https://doi.org/10.1101/514943; this version posted January 9, 2019. The copyright holder for this preprint (which was not certified by peer review) is the author/funder, who has granted bioRxiv a license to display the preprint in perpetuity. It is made available under aCC-BY-ND 4.0 International license.

35 – Underhill D.M., Ozinsky A., Smith K.D. & Aderem A. Toll-like receptor-2 mediates mycobacteria-induced proinflammatory signaling in macrophages. *Proceedings of the National Academy of Sciences* **7**, 96(25): 14459-14463 (1999).

36 - Bafica, A. et al. TLR9 regulates Th1 responses and cooperates with TLR2 in mediating optimal resistance to *Mycobacterium tuberculosis*. *The Journal of Experimental Medicine* **202**, 1715–1724 (2005).

37 - Brites, D. & Gagneux, S. Co-evolution of *Mycobacterium tuberculosis* and *Homo sapiens*. *Immunological Reviews* **264**, 6–24 (2015).

38 - Lee, J. et al. Restricted dendritic cell and monocyte progenitors in human cord blood and bone marrow. *The Journal of Experimental Medicine* **212**, 385–399 (2015).

39 - Endele, M., Etzrodt, M. & Schroeder, T. Instruction of hematopoietic lineage choice by cytokine signaling. *Experimental Cell Research* **329**, 207–213 (2014)

40 - Jansen, J. H. Interleukin 6 is a permissive factor for monocytic colony formation by human hematopoietic progenitor cells. *Journal of Experimental Medicine* **175**: 1151–1154 (1992).

41 - Naranbhai, V. et al. Distinct Transcriptional and Anti-Mycobacterial Profiles of Peripheral Blood Monocytes Dependent on the Ratio of Monocytes: Lymphocytes. *EBioMedicine* **2**, 1619–1626 (2015).

42 - Hecker, M. et al. Interferon-beta therapy in multiple sclerosis: the short-term and long-term effects on the patients' individual gene expression in peripheral blood. *Molecular Neurobiology* **48**, 737–756 (2013).

43 - Novikov, A. et al. Mycobacterium tuberculosis Triggers Host Type I IFN Signaling To Regulate IL-1β Production in Human Macrophages. *The Journal of Immunology* **187**, 2540–2547 (2011).

44 - Mayer-Barber KD et al. Innate and adaptive interferons suppress IL-1α and IL-1β production by distinct pulmonary myeloid subsets during Mycobacterium tuberculosis infection. *Immunity* **35**, 1023-34 (2011).

45 – Ho, H. H. & Ivashkiv, L. B. Role of STAT3 in Type I Interferon Responses. *Journal of Biological Chemistry* **281**, 14111–14118 (2006).

46 – Lawrence, H.J. et al. Frequent co-expression of the HOXA9 and MEIS1 homeobox genes in human myeloid leukemias. *Leukemia* **13**, 1993-9 (1999).

47 – Assi, S. A. et al. Subtype-specific regulatory network rewiring in acute myeloid leukemia. *Nature Genetics* (2018).

48 - Manry, J. et al. Evolutionary genetic dissection of human interferons. *The Journal of Experimental Medicine* **208**, 2747–2759 (2011).

bioRxiv preprint doi: https://doi.org/10.1101/514943; this version posted January 9, 2019. The copyright holder for this preprint (which was not certified by peer review) is the author/funder, who has granted bioRxiv a license to display the preprint in perpetuity. It is made available under aCC-BY-ND 4.0 International license.

49 - Shaw, A. E. et al. Fundamental properties of the mammalian innate immune system revealed by multispecies comparison of type I interferon responses. *PLOS Biology* **15**, e2004086 (2017).

50 - Quach, H. et al. Genetic Adaptation and Neandertal Admixture Shaped the Immune System of Human Populations. *Cell* **167**, 643–656.e17 (2016).

51 - Enard, D. & Petrov, D. A. Evidence that RNA Viruses Drove Adaptive Introgression between Neanderthals and Modern Humans. *Cell* **175**, 360–371.e13 (2018).

52 - Hagai, T. et al. Gene expression variability across cells and species shapes innate immunity. *Nature* **563**, 197–202 (2018).

53 - Dannemann, M., Prüfer, K. & Kelso, J. Functional implications of Neandertal introgression in modern humans. *Genome Biology* **18**, (2017).

54 - Qi, H. et al. Toll-like receptor 1(TLR1) Gene SNP rs5743618 is associated with increased risk for tuberculosis in Han Chinese children. *Tuberculosis* **95**, 197–203 (2015).

55 - Daub, J. T. et al. Evidence for Polygenic Adaptation to Pathogens in the Human Genome. *Molecular Biology and Evolution* **30**, 1544–1558 (2013).

56 - Bakker, O. B. et al. Integration of multi-omics data and deep phenotyping enables prediction of cytokine responses. *Nature Immunology* **19**, 776–786 (2018).

57 - Wang, J. et al. Ratio of monocytes to lymphocytes in peripheral blood in patients diagnosed with active tuberculosis. *The Brazilian Journal of Infectious Diseases* **19**, 125–131 (2015).

58 - Hirahara, K. et al. Asymmetric Action of STAT Transcription Factors Drives Transcriptional Outputs and Cytokine Specificity. *Immunity* **42**, 877–889 (2015).

59 – Van Weyenbergh et al. Treatment of multiple sclerosis patients with interferon-beta primes monocyte-derived macrophages for apoptotic cell death. *Journal of Leukocyte Biology* **70**, 745-8 (2001).

60 - Menezes, S. et al. CD80+ and CD86+ B cells as biomarkers and possible therapeutic targets in HTLV-1 associated myelopathy/tropical spastic paraparesis and multiple sclerosis. *Journal of Neuroinflammation* **11**, 18 (2014).

61 - Norris, B. A. & Ernst, J. D. Mononuclear cell dynamics in M. tuberculosis infection provide opportunities for therapeutic intervention. PLOS Pathogens 14, e1007154 (2018).

62 - Joosten, S. A. et al. Mycobacterial growth inhibition is associated with trained innate immunity. *Journal of Clinical Investigation* **128**, 1837–1851 (2018).

63 - Mitroulis, I. et al. Modulation of Myelopoiesis Progenitors Is an Integral Component of Trained Immunity. *Cell* **172**, 147–161.e12 (2018).

bioRxiv preprint doi: https://doi.org/10.1101/514943; this version posted January 9, 2019. The copyright holder for this preprint (which was not certified by peer review) is the author/funder, who has granted bioRxiv a license to display the preprint in perpetuity. It is made available under aCC-BY-ND 4.0 International license.

64 - Arts, R. J. W. et al. BCG Vaccination Protects against Experimental Viral Infection in Humans through the Induction of Cytokines Associated with Trained Immunity. *Cell Host & Microbe* **23**, 89–100.e5 (2018).

65 - Zhang, G. et al. Allele-Specific Induction of IL-1β Expression by C/EBPβ and PU.1 Contributes to Increased Tuberculosis Susceptibility. *PLOS Pathogens* **10**, e1004426 (2014).

66 - Zhang, G. et al. A Functional Single-Nucleotide Polymorphism in the Promoter of the Gene Encoding Interleukin 6 Is Associated With Susceptibility to Tuberculosis. *The Journal of Infectious Diseases* **205**, 1697–1704 (2012)

67 - Zhang, G. et al. A proline deletion in IFNAR1 impairs IFN-signaling and underlies increased resistance to tuberculosis in humans. *Nature Communications* **9**, (2018).

68 - Bustamante, J. et al. Mendelian susceptibility to mycobacterial disease: Genetic, immunological, and clinical features of inborn errors of IFN-γ immunity. *Seminars in Immunology* **26**, 454–470 (2014).

69 - Antonelli, L. R. V. et al. Intranasal Poly-IC treatment exacerbates tuberculosis in mice through the pulmonary recruitment of a pathogen-permissive monocyte/macrophage population. *Journal of Clinical Investigation* **120**, 1674–1682 (2010).

70 – Akira, S. et al. A nuclear factor for IL-6 expression (NF-IL6) is a member of a C/EBP family. *The EMBO Journal* **9**, 1897-906 (1990).

71 - Lefrançais E et al. The lung is a site of platelet biogenesis and a reservoir for haematopoietic progenitors. *Nature* **544**,105-109 (2017).

72 - Okada, M. et al. Anti-IL-6 Receptor Antibody Causes Less Promotion of Tuberculosis Infection than Anti-TNF- Antibody in Mice. *Clinical and Developmental Immunology* **2011**, 1–9 (2011).

73 - Zumla A et al. Potential of immunomodulatory agents as adjunct host-directed therapies for multidrug-resistant tuberculosis. *BMC Medicine* **14**:89 (2016).

74 - Yamashiro LH et al. Isoniazid-induced control of Mycobacterium tuberculosis by primary human cells requires interleukin-1 receptor and tumor necrosis factor. *European Journal of Immunology* **46**, 1936-47 (2016).

75 - Patro, R., Duggal, G., Love, M. I., Irizarry, R. A. & Kingsford, C. Salmon provides fast and bias-aware quantification of transcript expression. *Nature Methods* **14**, 417–419 (2017).

76 - Lummertz da Rocha, E. et al. Reconstruction of complex single-cell trajectories using CellRouter. *Nature Communications* **9**, (2018).

77 – Love, M. I., Huber, W. & Anders, S. Moderated estimation of fold change and dispersion for RNA-seq data with DESeq2. *Genome Biology* **15**, (2014).

bioRxiv preprint doi: https://doi.org/10.1101/514943; this version posted January 9, 2019. The copyright holder for this preprint (which was not certified by peer review) is the author/funder, who has granted bioRxiv a license to display the preprint in perpetuity. It is made available under aCC-BY-ND 4.0 International license.

Figure legends

Fig. 1 | *Mtb* H37Rv infects human CD34$^+$ cells and proliferates in cell cultures in vitro. PBMC from healthy donors were exposed to Syto24-labeled *Mtb* H37Rv (MOI3, Supplementary Fig. 1a) for 4h. **a,** Representative flow cytometry contour plots of gating strategy to analyze *Mtb* association within PBMC CD34$^+$ cells. **b,** Live Lin$^-$CD34$^+$ events gated in (a) were analyzed for *Mtb*-Syto24 MFI. Black line: Uninfected control. Blue, orange and purple lines represent samples from three different donors. **c,** Frequencies and **d,** MFI of *Mtb*-Syto24$^+$ events within CD34$^+$ or CD14$^+$ cell populations. Results are means ± SEM of data pooled from 3 independent experiments, n = 10 healthy donors**. e,** Purified CB CD34$^+$ cells were exposed to *Mtb* H37Rv (MOI3) for different time points and CFUs from cell culture lysates were enumerated in 7H10 media. Results are means ± SEM of data pooled from 5 independent experiments, ***p≤0.001 between experimental and control groups. **f,** Kinyoun staining of CD34$^+$ cells after 1d and 5d of infection. Arrows indicate cells associated with bacilli. Experiments shown are representative of three performed. **g,** Representative Giemsa staining of CD34$^+$ cells of a 5d culture. Arrow indicates cytoplasm-rich monocytoid cells in *Mtb*-infected cultures. Experiments shown are representative of three performed.

Fig. 2 | Live *Mtb* induces human CD34$^+$ cells towards myeloid differentiation in vitro*.* Purified CD34$^+$ cells from healthy donors (Stemcell technologies, n = 3) were exposed to *Mtb* H37Rv (MOI3) for different time points and mRNA-seq was performed as described in methodology section. **a,** Heatmap of the mRNA expression (z-score) of transcription factors involved in cell lineage commitment[24]. **b,** Signature score of data

bioRxiv preprint doi: https://doi.org/10.1101/514943; this version posted January 9, 2019. The copyright holder for this preprint (which was not certified by peer review) is the author/funder, who has granted bioRxiv a license to display the preprint in perpetuity. It is made available under aCC-BY-ND 4.0 International license.

from **a** by employing CellRouter analysis. **c,** Heatmap from mRNA data of uninfected vs *Mtb* infected cultures analyzed by CellNet as described in methodology section. **d,** Purified CB $CD34^+$ cells were exposed to *Mtb* H37Rv (MOI3) for 5 days and flow cytometry was performed. Graph represents frequencies of $CD11b^+$ events in uninfected (open circles) vs *Mtb*-infected cultures (blue circles) from four independent experiments. ** $p \leq 0.01$ between experimental and control groups. **e**, Purified CB $CD34^+$ cells were exposed to *Mtb* H37Rv, Heat-killed (HK) *Mtb* H37Rv or *Mtb* clinical isolate 267 (MOI3) for 5 days and flow cytometry with the gating strategy was performed. **f,** Representative contour plots show frequencies of $CD4^+CD64^+$ events within $CD34^+$ events. $CD34^+CD4^+CD64^+$ events of polled data from **f** were plotted to generate bar graphs **g** and **h.** Results are means ± SEM of data pooled from 4 independent experiments **g** and 2 independent experiments **h.** ** $p \leq 0.01$ between experimental and control groups.

Fig. 3 | *Mtb* infection increases monocyte output from $CD34^+$ cells in vitro. Purified CB $CD34^+$ cells were exposed to *Mtb* H37Rv or HK *Mtb* H37Rv (MOI3) for 10 days and flow cytometry was employed to determine the frequencies of **a,** monocytes ($CD14^+$), **b,** neutrophils ($CD16^+CD66b^+$), **c,** megakaryocytes/platelets ($CD41a^+$) and **d,** classical myeloid dendritic cells ($BDCA1^+CD14^{low}$) in uninfected and *Mtb*-infected $CD34^+$ cell cultures. Graphs show frequencies of **e,** $CD14^+$, **f,** $CD16^+CD66b^+$, **g,** $CD41a^+$ and **h,** $BDCA1^+CD14^{low}$ events in uninfected (open circles), *Mtb*-infected (blue diamonds) or HK *Mtb*-exposed (red diamonds) cell cultures at day 10. Each symbol represents one individual experiment. Results are means ± SEM of data pooled from 3 - 9 independent experiments. ** $p \leq 0.01$ between experimental and control groups. **i,** Histograms show the expression of CD11b, HLA-DR, CD64 and CD16 in $CD14^+$ events from **a**. Black dashed lines: Uninfected control. Blue solid lines: *Mtb*-infected group. Data representative of 5 independent experiments. **j,** Frequency of $CD14^+CD16^+$ events in

bioRxiv preprint doi: https://doi.org/10.1101/514943; this version posted January 9, 2019. The copyright holder for this preprint (which was not certified by peer review) is the author/funder, who has granted bioRxiv a license to display the preprint in perpetuity. It is made available under aCC-BY-ND 4.0 International license.

Mtb-exposed cell cultures after 10d. Contour dot plot of $CD14^+CD16^+$ frequencies from one representative donor. Open circles: Uninfected control. Blue circles: *Mtb*-infected group. Each symbol represents an individual experiment. Pooled data of eight independent experiments, n = 5 different donors. p=0.076 between experimental and control groups.

Fig. 4 | *Mtb* enhances IL-6R-mediated myeloid differentiation in vitro. Purified CB $CD34^+$ cells were exposed to *Mtb* H37Rv (MOI3) for different time points and mRNA-seq was performed as described in methodology section. **a,** Heatmap (z-score) of differentially expressed interleukin receptor genes. **b,** Heatmap (z-score) of differentially expressed interleukin genes. Shown is average mRNA expression of three different donors from two independent experiments. **c,** Supernatant IL-6 measurements from unexposed or *Mtb*-exposed CB $CD34^+$ cell cultures at day 1 and 5 p.i. Open circle: uninfected control. Blue circle: *Mtb*-infected group. Results are means ± SEM of data pooled from 8 independent experiments. ** p≤0.05 between 1d experimental and control groups. Purified CB $CD34^+$ cells were treated with **d,** anti-IFNAR2 (1 µg/ml) or **e,** anti-IFN-γ (10 µg/ml) and then exposed to *Mtb* H37Rv (MOI3) during 10d for determination of $CD14^+$ monocyte frequencies. Results are means ± SEM of data pooled from 2 independent experiments**. f,** Representative contour plots of $CD14^+$ monocytes in $CD34^+$ cell cultures exposed to *Mtb*, in the presence or absence of anti-IL6R (Tocilizumab, 1 µg/ml) for 10d. **g,** Results shown are means ± SEM of data pooled from 3 independent experiments from **f.** **p≤0.01 between uninfected and *Mtb* group and #p≤0.05 between *Mtb* and *Mtb*+anti-IL6R-treated group. **h,** Results shown are means ± SEM of data pooled from 3 independent experiments showing frequency of $CD66^+CD16^+$ neutrophils in *Mtb*-infected cell cultures in the presence or absence of anti-IL6R. $CD34^+$ cell cultures were treated as in **d-f** with **i,** anti-IL6R, **j,** anti-IFNAR2 and **k,** anti-IFN-γ and then

bioRxiv preprint doi: https://doi.org/10.1101/514943; this version posted January 9, 2019. The copyright holder for this preprint (which was not certified by peer review) is the author/funder, who has granted bioRxiv a license to display the preprint in perpetuity. It is made available under aCC-BY-ND 4.0 International license.

exposed to *Mtb* CFUs for different time points and CFU enumerated as described in Material and Methods. Results are means ± SEM of data pooled from 4 independent experiments. **p≤0.01 between *Mtb* and *Mtb*+anti-IL6R at 7d.

Fig. 5 | An *IL6/IL6R/STAT3/CEBPB* gene module is enriched in active TB transcriptome and proteome and correlates with myeloid differentiation and disease severity. a, Upper panel: upstream regulators significantly enriched by causal Ingenuity Pathway Analysis (IPA) in monocyte transcriptomes from patients with active TB (GSE19443), ranked by activation z-score, p-values are corrected for genome-wide testing (FDR). Lower panel: IRF1 and STAT1 are the top upstream regulators shared between the Berry et al. TB disease signature (GSE19435, GSE19439, GSE19444), the IL6/STAT3 pathway (Hallmark GSEA) and the "human in vivo IFN-β signature" (GSEA HECKER_IFNB1_TARGETS). **b,** Upper panel: overlap between the Berry et al. TB disease signature, IL6/STAT3 pathway (GSEA) and the active TB plasma proteomic signature[41]. Lower panel: significant STRING protein-protein interaction network ($p<10^{-16}$) for IFN/IL6 shared genes (green marbles) and IL6/STAT3 genes (red marbles), clustering separately by k-means. **c,** Upper panel: significant linear increase over time before active TB diagnosis in plasma proteome[41] for "CD34/myeloid" (yellow), "IL6/STAT3" (orange) and "IFN/IL6-shared" (blue) clusters found in **b**. Lower panel: monocyte/lymphocyte (ML) ratio gene set members defined by Narabhai et al.[42] over time before active TB diagnosis in plasma proteome[41]. **d,** Upper panel: increased "IL6/STAT3" cluster protein expression precedes monocyte expansion markers (ML ratio gene set) in the TB plasma proteome. Lower panel: data as in **d** shows significant higher fold-changes for "IL6/STAT3" vs. "IFN/IL6-shared" cluster members. **e,** Transcription factor enrichment analysis (GSEA) of differentially expressed genes (determined by RNA-seq) in *Mtb*-exposed $CD34^+$ cells in vitro (n = 3 donors). **f,** Multi-cohort transcription

bioRxiv preprint doi: https://doi.org/10.1101/514943; this version posted January 9, 2019. The copyright holder for this preprint (which was not certified by peer review) is the author/funder, who has granted bioRxiv a license to display the preprint in perpetuity. It is made available under aCC-BY-ND 4.0 International license.

factor enrichment analysis (GSEA) of large transcriptomic data sets shows overlap between TB active disease signature[18], in vitro CD34$^+$ *Mtb* signature at 24h, in vivo monocyte expansion (ML ratio)[42], disseminated TB (lymph node, GSE63548), as well as TB patients with BCG vaccine failure (GSE20716). **g,** Transcriptional analysis of whole blood shows significant correlation of *CEBPB* transcripts with *IL6R* and *STAT3* transcript levels, mycobacterial positivity in sputum smears, C-reactive protein (CRP), tissue damage (Modal X-ray grade), symptom count as well as systemic clinical parameters (lymphocyte count, albumin and haemoglobin levels), in patients with tuberculosis. Results shown are from UK cohort described in ref. 18 (n = 30 patients with latent and active TB) P-value<0.05, ** p-value<0.01, *** p-value<0.001, **** p-value<0.0001.

Fig. 6 | Evolutionary recent and human-specific genetic adaptation link *IL6/IL6R/CEBP* axis with monocyte expansion and TB pathogenesis. **a,** Upper panel: STRING protein-protein interaction networks centred around *CEBPB* (left) and *IL6R* (right, both $p<10^{-16}$), k-means clustering shows *CEBPA, CEBPB and CEBPD* myeloid TF (green marbles, left panel) and "IFN/IL6 shared" genes (green marbles, right panel) form separate clusters. Lower panel: Heat map showing *CEBPB* vs. *IL6R* networks generated by STRING co-occurrence protein conservation scores across primates, mammals, birds and reptiles. Note only *CEBPB and CEBPA* differ strongly among hominids, while *CEBPA-CEBPB-CEBPD* vary significantly throughout primate and mammalian evolution, as compared to highly conserved *STAT3/STAT1* amino acids. **b,** Highly conserved type I IFN upregulation of "IFN/IL6-shared" genes from humans to birds (derived from http://isg.data.cvr.ac.uk/), as compared to "IL6/STAT3" and "CD34/myeloid differentiation" genes. **c,** *CEBPB* displays high variation in type I IFN transcriptional regulation across human-mammalian-bird

bioRxiv preprint doi: https://doi.org/10.1101/514943; this version posted January 9, 2019. The copyright holder for this preprint (which was not certified by peer review) is the author/funder, who has granted bioRxiv a license to display the preprint in perpetuity. It is made available under aCC-BY-ND 4.0 International license.

evolution. *Inset, CEBPB* and *CEBPD* selectively acquired type I IFN upregulation in humans (filled circles); ** p-value<0.01 and * p-value<0.05 represent *CEBPB* and *CEBPD* values, respectively for humans versus the other species. **d,** Left panel: both IFN-regulated and IL6-regulated transcripts display significantly higher effect size on monocyte/lymphocyte (ML) ratio as compared to all other ML ratio gene set members. Right panel: IL6-regulated transcripts have significantly higher effect sizes on absolute monocyte counts, as compared to IFN-regulated transcripts (p<0.05). **e,** Left panel: overlap between human genes with significant Neandertal introgression, genes differentially expressed in *Mtb*-exposed $CD34^+$ cells ($CD34^+$ DE) and the "ML ratio" gene set. Right panel: *OAS1, OAS2* and *MT2A* transcripts presented significantly higher effect sizes upon ML ratios, corresponding to monocyte expansion, as compared to other introgressed genes (p<0.05) and to all other genes shown to regulate ML ratio in vivo (p<0.001). **f,** Compiled functional, proteomic, transcriptomic and genomic evidence for an IL6/IL6R/CEBP gene module linking CD34+ myeloid differentiation to TB pathogenesis and disease severity. For enrichment analysis (GSEA) and differential gene expression, ranks were determined as 0-1-2-3 according to quartiles; z-scores were obtained from Daub et al.[55] p-value<0.05, ** p-value<0.01, *** p-value<0.001, **** p-value<0.0001. **g,** Proposed model for *Mtb* hijacking of IL-6-mediated $CD34^+$ myeloid differentiation pathways using an IFN/IL6 feed-forward loop (details in the text).

Supplementary Figure Legends

S1 – *Mtb*-$CD34^+$ interactions and signaling pathways associated with $CD34^+$ cell differentiation. a, Gating strategy demonstrating H37Rv stained for Syto24 as measured through the FL1 channel. **b,** Confocal microscopy showing a $CD34^+$ cell infected with Syto24-stained H37Rv. Nuclei = DAPI/blue. *Mtb* = Syto24/green. **c,** Heat map showing z-score values of 180 transcription factors[24] expressed by $CD34^+$ cells

bioRxiv preprint doi: https://doi.org/10.1101/514943; this version posted January 9, 2019. The copyright holder for this preprint (which was not certified by peer review) is the author/funder, who has granted bioRxiv a license to display the preprint in perpetuity. It is made available under aCC-BY-ND 4.0 International license.

exposed to *Mtb* (MOI3) at days 1,3 and 5 post-infection. **d,** Enrichment of Reactome pathways based on gene signatures derived from each experimental condition. Enrichment of Reactome pathways based on gene signatures derived from each experimental condition. Gene signatures were composed by genes with log2 fold change > 0.75 when comparing one experimental condition versus all others. The size and color of the circles are proportional to the -log10 of the adjusted p-value.

S2 – *Mtb* induces myeloid progenitors in bone marrow and peripheral blood mononuclear cells. a, Frequencies of $CD10^{+}CD34^{+}$ and $CD41a^{+}CD34^{+}$ cells in uninfected vs *Mtb*-infected cell cultures. Dot plots of **b,** bone marrow and **c,** peripheral blood samples from 2-4 healthy subjects showing frequencies of $CD4^{+}CD64^{+}CD34^{+}$ and $CD38^{+}HLADR^{+}CD34^{+}$ cells in uninfected vs *Mtb*-infected cell cultures.

S3 – Purified mycobacterial agonists partially activate $CD34^{+}$ cells. a, CD34+ cells were exposed to AraLam (10 μg/ml) or gDNA (10 μg/ml) and 5 days later, CD34+ cells were gated and CD38, HLADR, CD4 and CD64 MFI calculated. Cell death analysis by means of **b,** frequencies of cell permeability dye (FVS+) and **c,** LDH quantities detected in the supernatants from uninfected of *Mtb*-exposed $CD34^{+}$ cell cultures 5 dpi. **d,** Frequencies of CD14+ cells during 10-day exposure to a clinical isolate of *Mtb*. **e,** The erythroid cell marker CD235a was measured by flow cytometry in *Mtb*-exposed and control $CD34^{+}$ cells 10 dpi.

S4 – IL6/IFN gene expression and transcription factor activation during myeloid differentiation by *Mtb*-exposed $CD34^{+}$ cells. $CD34^{+}$ cells were exposed to *Mtb* (MOI3) and at days 1, 3 and 5 p.i., qPCR was performed for quantification of **a,** IL6/IFN

bioRxiv preprint doi: https://doi.org/10.1101/514943; this version posted January 9, 2019. The copyright holder for this preprint (which was not certified by peer review) is the author/funder, who has granted bioRxiv a license to display the preprint in perpetuity. It is made available under aCC-BY-ND 4.0 International license.

cytokines and **b,** ISGs and IL-6-induced genes. **c,** $CD34^+$ cells were stimulated with or without recombinant IL-6 for 5 days and frequencies of $CD4^+CD64^+CD34^+$ cells were measured by flow cytometry. $CD66b^+CD16^+$ neutrophil frequencies in 10-day culture of *Mtb*-exposed $CD34^+$ treated with **d,** anti-IFNAR2 (1 µg/ml) or **e,** anti-IFN-γ (10 µg/ml) blocking antibodies. **f,** $CD41^+$ megakariocytes**, g,** $CD235^+$ erythrocytes and **h,** $BDCA1^+$CD14low myeloid DC frequencies in 10-day culture of *Mtb*-exposed $CD34^+$ treated with anti-IL-6R blocking or control antibodies. **i,** Western blotting for pSTAT1 (Y701), total STAT1, C/EBPα, C/EBPβ and actin was performed as described in the methodology.

S5 – ISG/CEBP gene expression and regulation during myeloid differentiation by *Mtb*-exposed $CD34^+$ cells. a, Purified CB $CD34^+$ cells were exposed to *Mtb* H37Rv (MOI3) for different time points. Heat maps showing z-score values of *CEBP* family members expressed by $CD34^+$ cells exposed to *Mtb* (MOI3) at different time points. **b**, Primary dermal fibroblasts from humans, macaques and mice were stimulated for 8h in vitro with dsRNA analog (polyI:C) and *CEBP* family member transcript levels were quantified by RNAseq (expressed as fold-change over unstimulated cells). Raw data obtained from Hagai et al.[52] (https://scb.sanger.ac.uk/#/base/main). **c,** Overlap between conserved mammalian ISGs (as in Fig. 6 c,d), the "IL6/STAT3 pathway" and the "ML ratio" gene set defined by Narabhai et al.[42] (upper right panel). **d**, Data plotted as genetic factor, which is the variance of cytokine secretion explained by genetics corrected for age and gender[56]. from monocyte-derived IL-6, TNF, IL-1β and lymphocyte-derived IL-17, IL-22 and IFN-γ. Cells were exposed to bacterial and viral stimuli (LPS, PolyI:C, Influenza, *E. coli, B. burgdorferi, M. tb, C. burnetii, S. aureus*) and monocyte-derived IL-6, TNF, IL-1β as well as lymphocyte-derived IL-17, IL-22 and IFN-γ measured[56]. **e,**

bioRxiv preprint doi: https://doi.org/10.1101/514943; this version posted January 9, 2019. The copyright holder for this preprint (which was not certified by peer review) is the author/funder, who has granted bioRxiv a license to display the preprint in perpetuity. It is made available under aCC-BY-ND 4.0 International license.

Purified CB $CD34^+$ cells were exposed to *Mtb* H37Rv (MOI3) for different time points. Heat maps showing z-score values of ISGs expressed by $CD34^+$ cells exposed to *Mtb* (MOI3) at different time points. **f**, Lymphocyte and monocyte counts, as well as monocyte/lymphocyte (ML) ratio before and after 3 months of IFN-β treatment in 7 MS patients previously described as IFN-β responders[59,60].

bioRxiv preprint doi: https://doi.org/10.1101/514943; this version posted January 9, 2019. The copyright holder for this preprint (which was not certified by peer review) is the author/funder, who has granted bioRxiv a license to display the preprint in perpetuity. It is made available under aCC-BY-ND 4.0 International license.

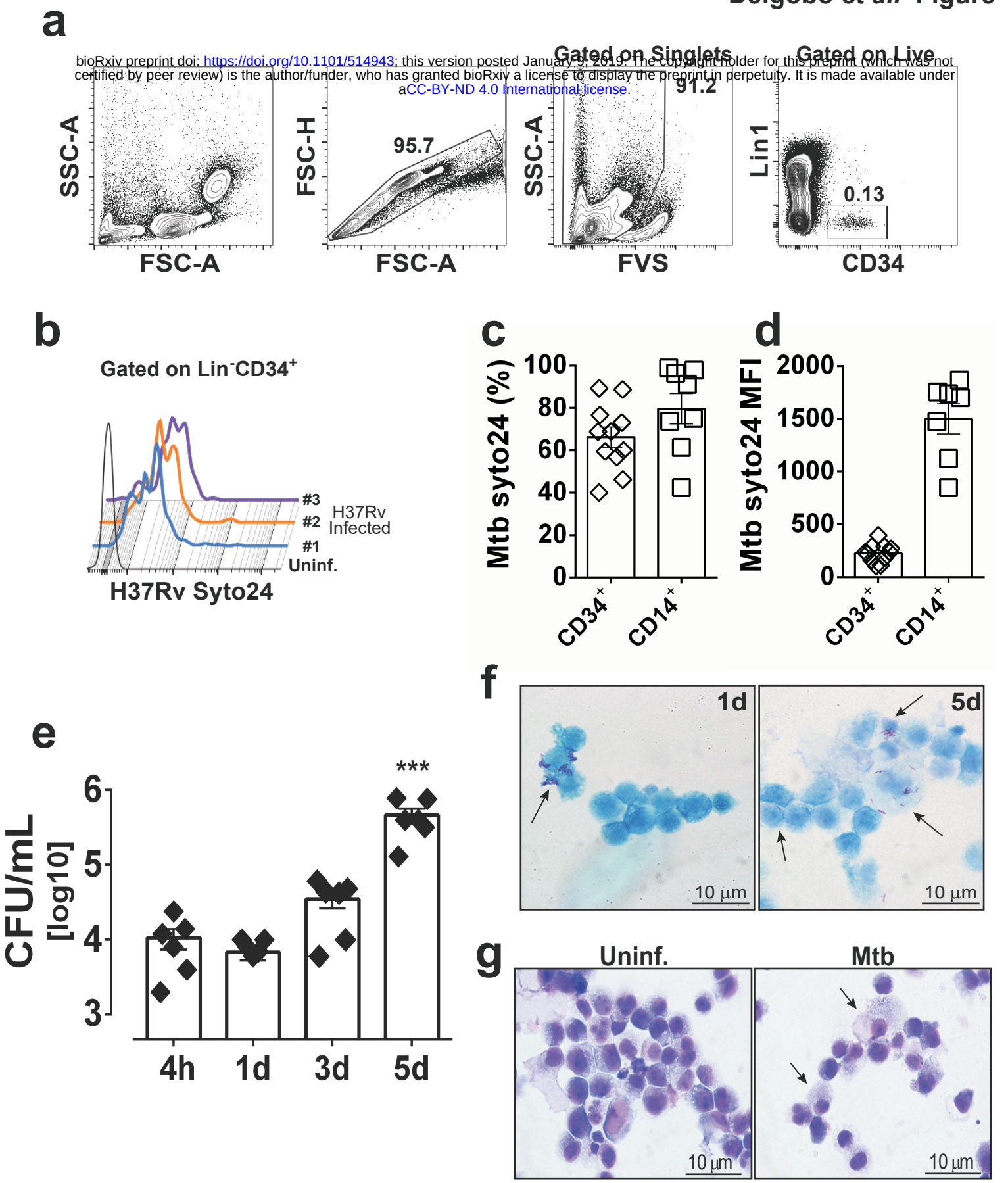

bioRxiv preprint doi: https://doi.org/10.1101/514948, this version posted January 9, 2019. The copyright holder for this preprint (which was not certified by peer review) is the author/funder, who has granted bioRxiv a license to display the preprint in perpetuity. It is made available under aCC-BY-ND 4.0 International license.

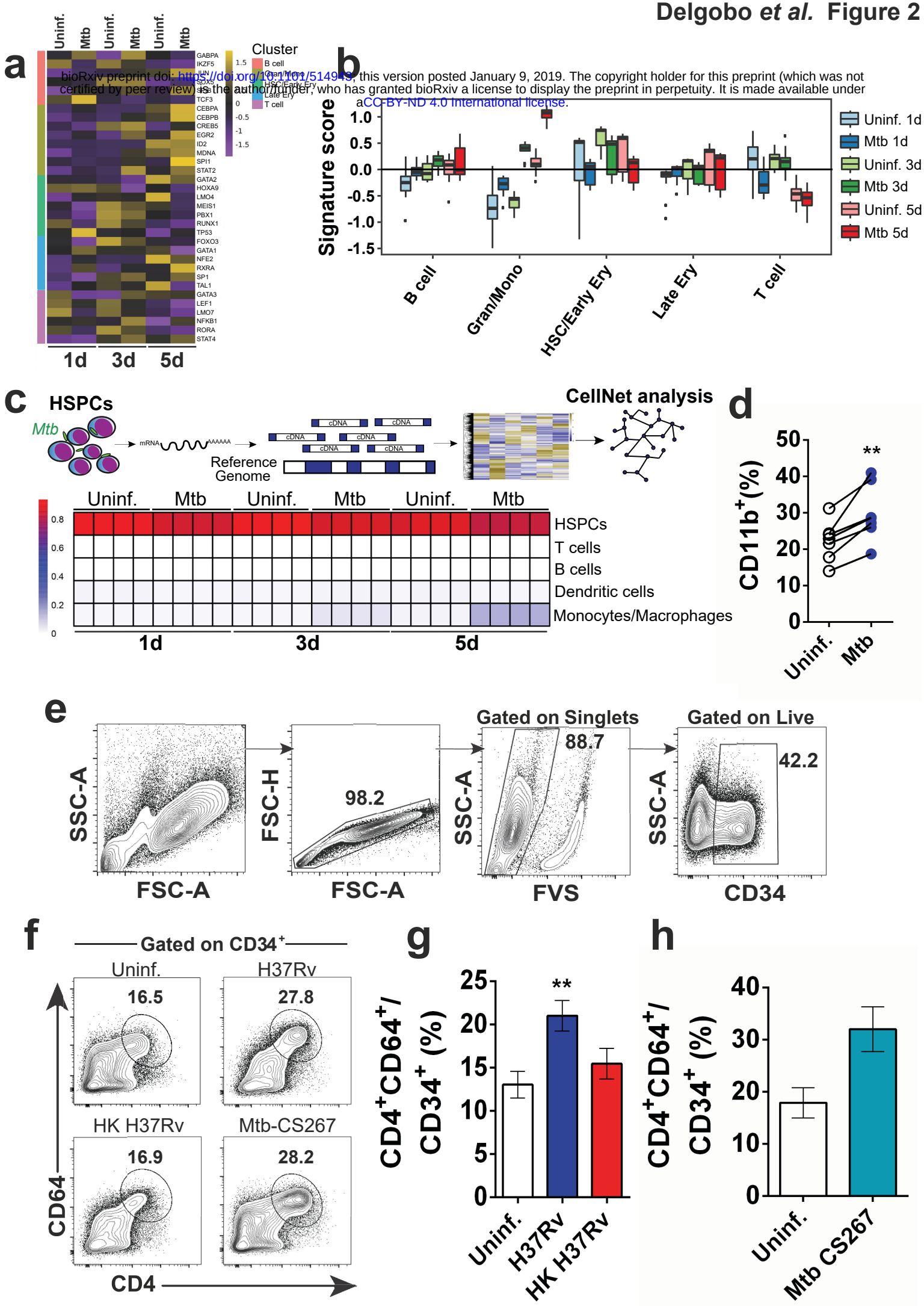

bioRxiv preprint doi: https://doi.org/10.1101/514943; this version posted January 9, 2019. The copyright holder for this preprint (which was not certified by peer review) is the author/funder, who has granted bioRxiv a license to display the preprint in perpetuity. It is made available under aCC-BY-ND 4.0 International license.

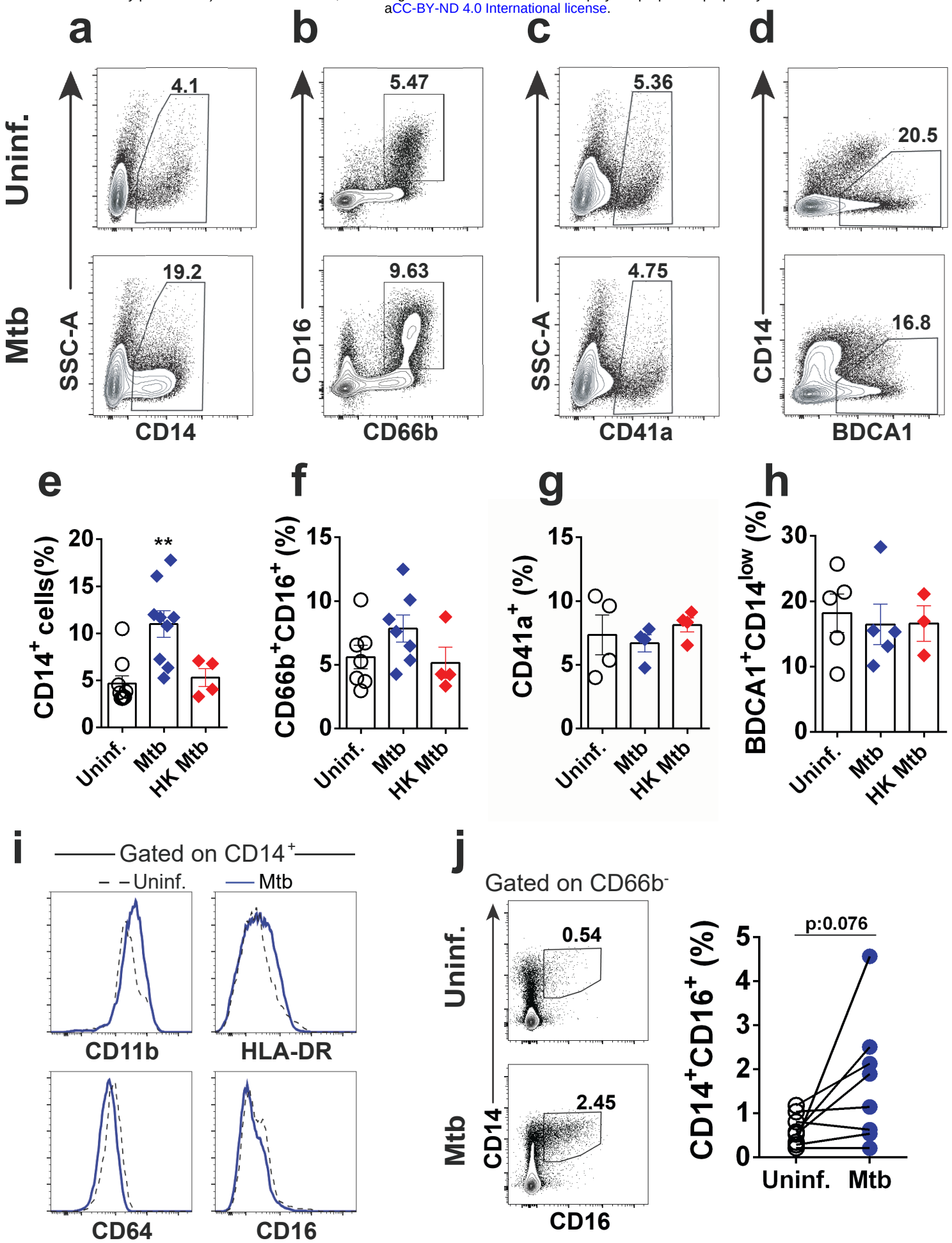

bioRxiv preprint doi: https://doi.org/10.1101/514943; this version posted January 9, 2019. The copyright holder for this preprint (which was not certified by peer review) is the author/funder, who has granted bioRxiv a license to display the preprint in perpetuity. It is made available under aCC-BY-ND 4.0 International license.

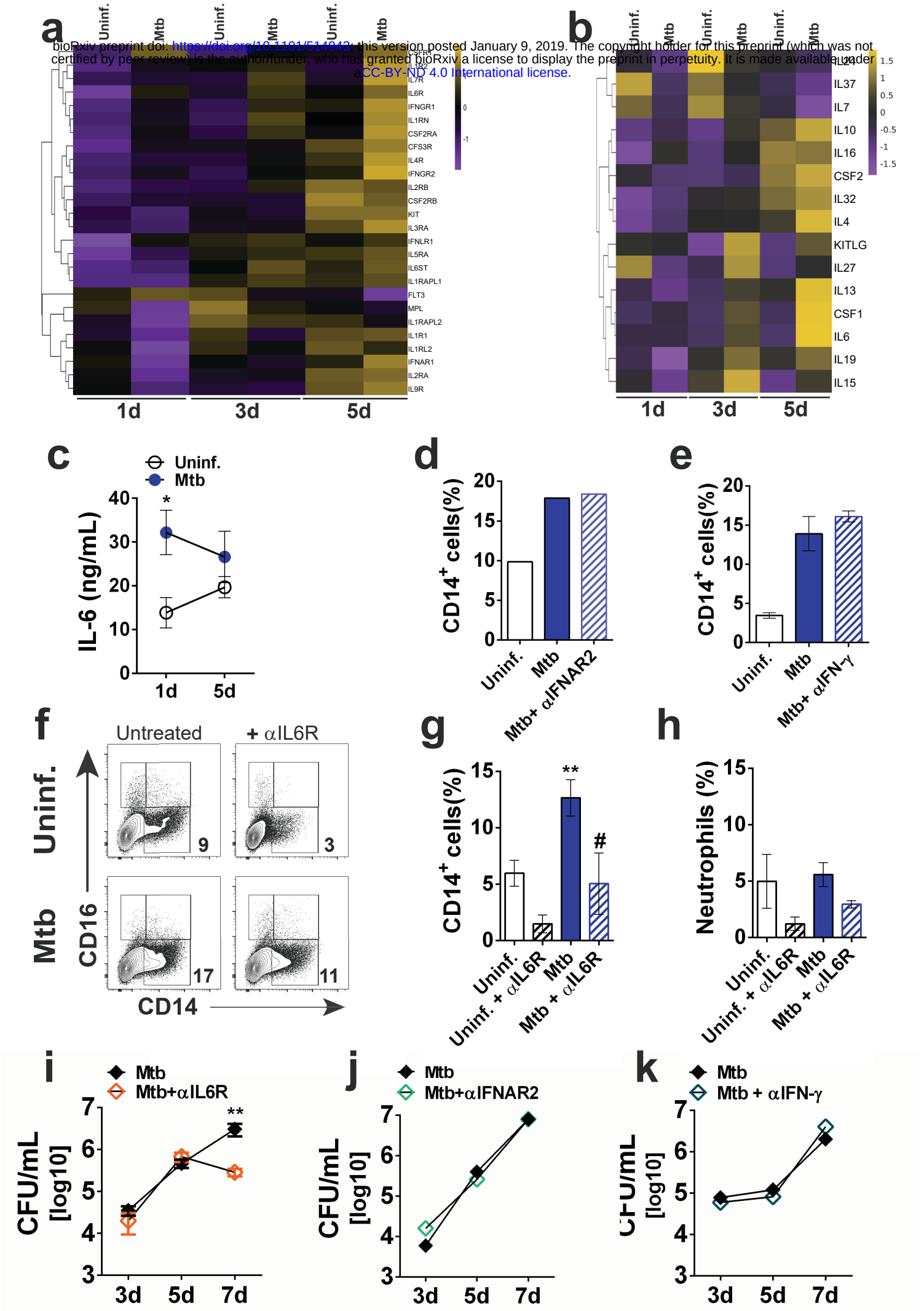

bioRxiv preprint doi: https://doi.org/10.1101/514943; this version posted January 9, 2019. The copyright holder for this preprint (which was not certified by peer review) is the author/funder, who has granted bioRxiv a license to display the preprint in perpetuity. It is made available under aCC-BY-ND 4.0 International license.

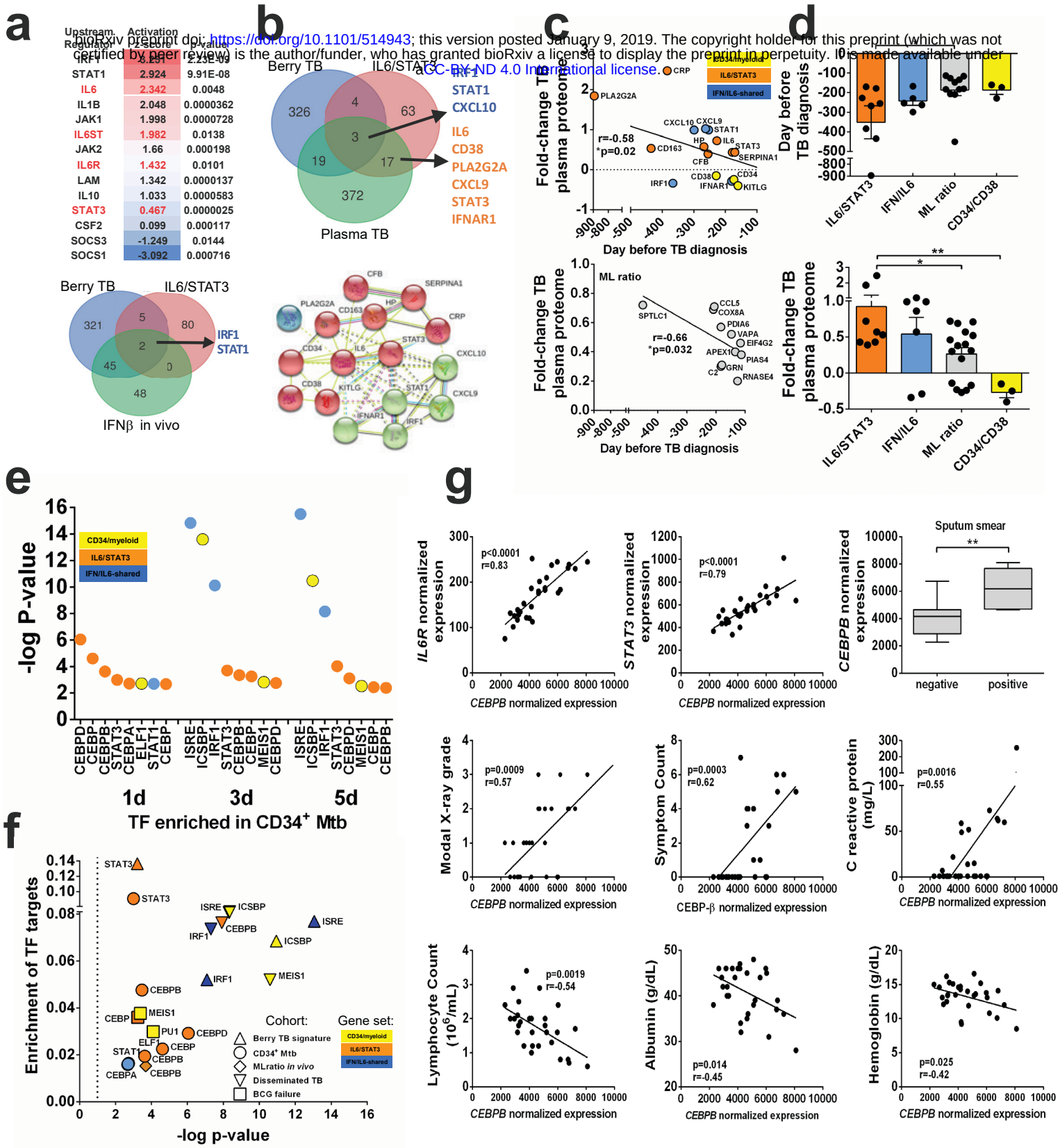

bioRxiv preprint doi: https://doi.org/10.1101/514943; this version posted January 9, 2019. The copyright holder for this preprint (which was not certified by peer review) is the author/funder, who has granted bioRxiv a license to display the preprint in perpetuity. It is made available under aCC-BY-ND 4.0 International license.

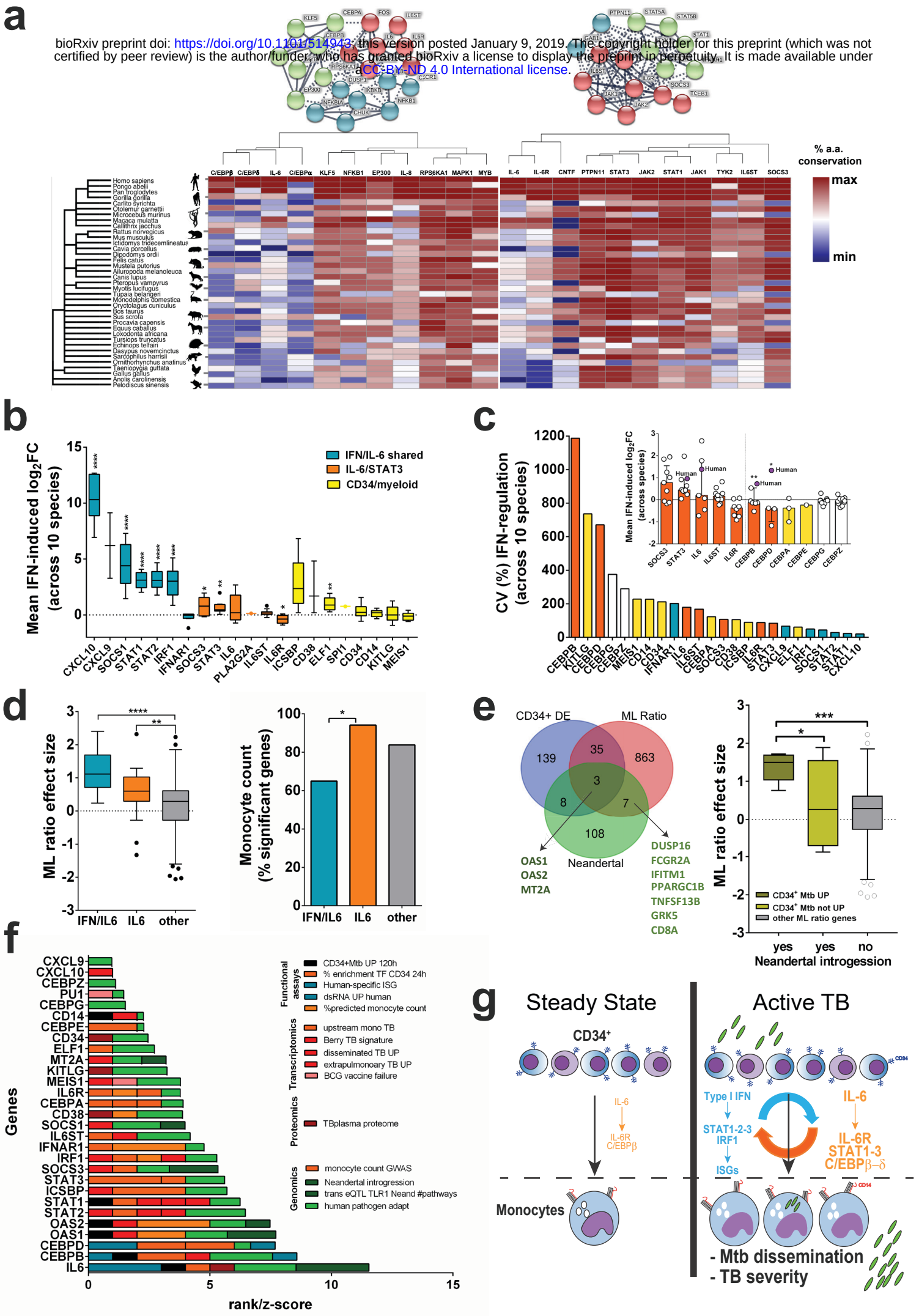

bioRxiv preprint doi: https://doi.org/10.1101/514943; this version posted January 9, 2019. The copyright holder for this preprint (which was not certified by peer review) is the author/funder, who has granted bioRxiv a license to display the preprint in perpetuity. It is made available under aCC-BY-ND 4.0 International license.

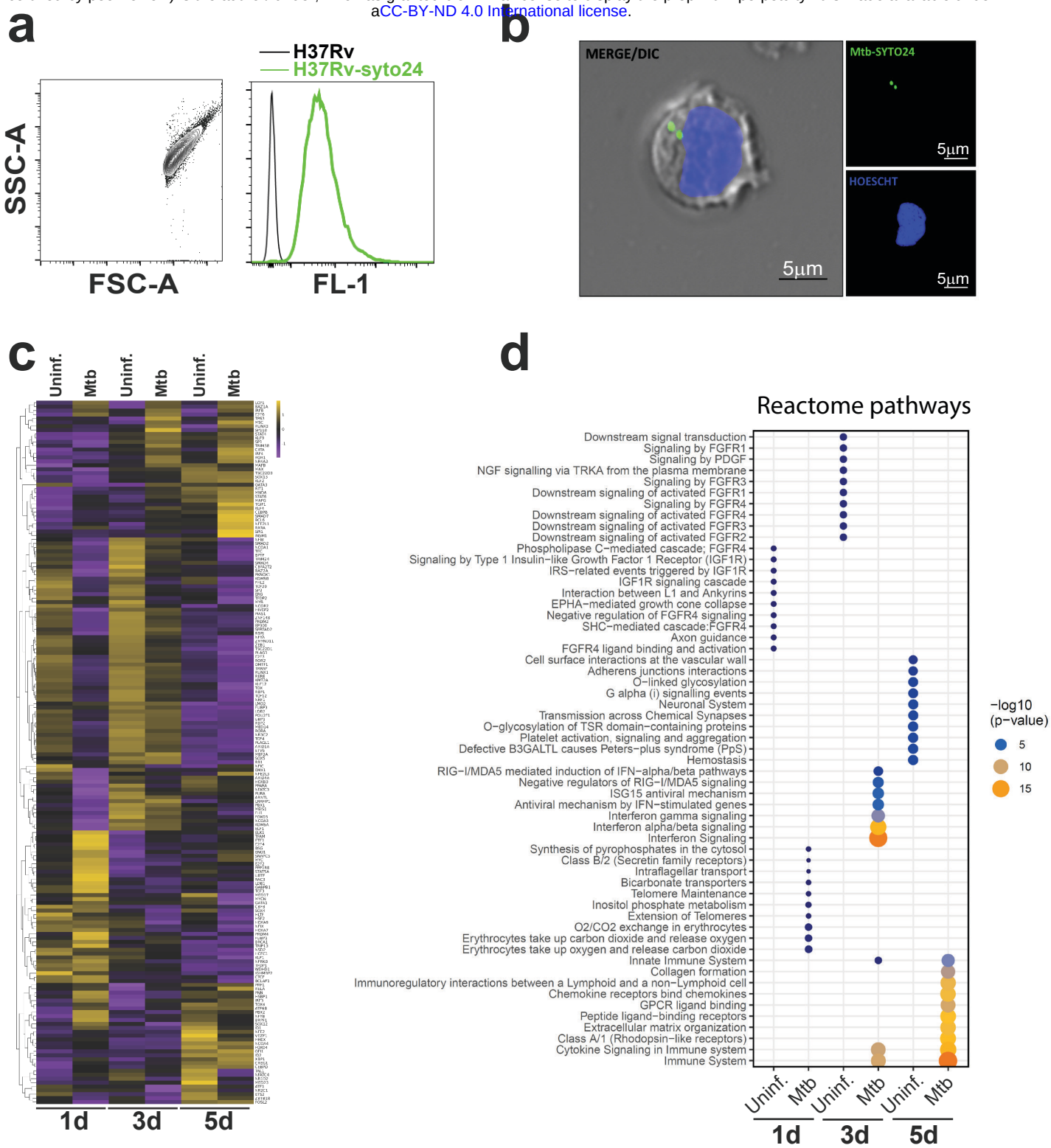

bioRxiv preprint doi: https://doi.org/10.1101/514943; this version posted January 9, 2019. The copyright holder for this preprint (which was not certified by peer review) is the author/funder, who has granted bioRxiv a license to display the preprint in perpetuity. It is made available under aCC-BY-ND 4.0 International license.

a

Gated on CD34$^+$

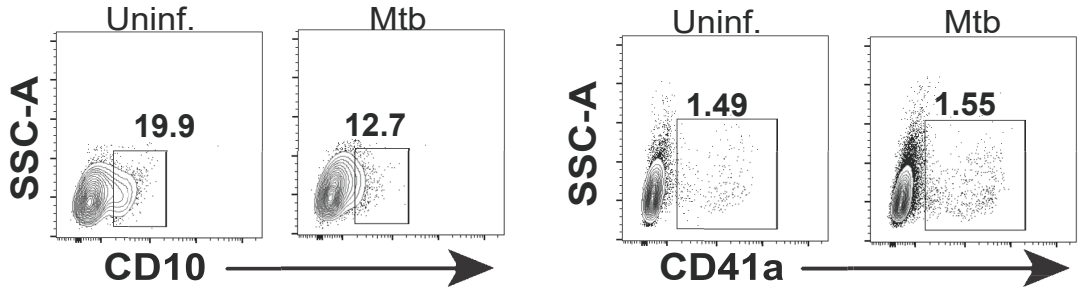

b

Bone marrow

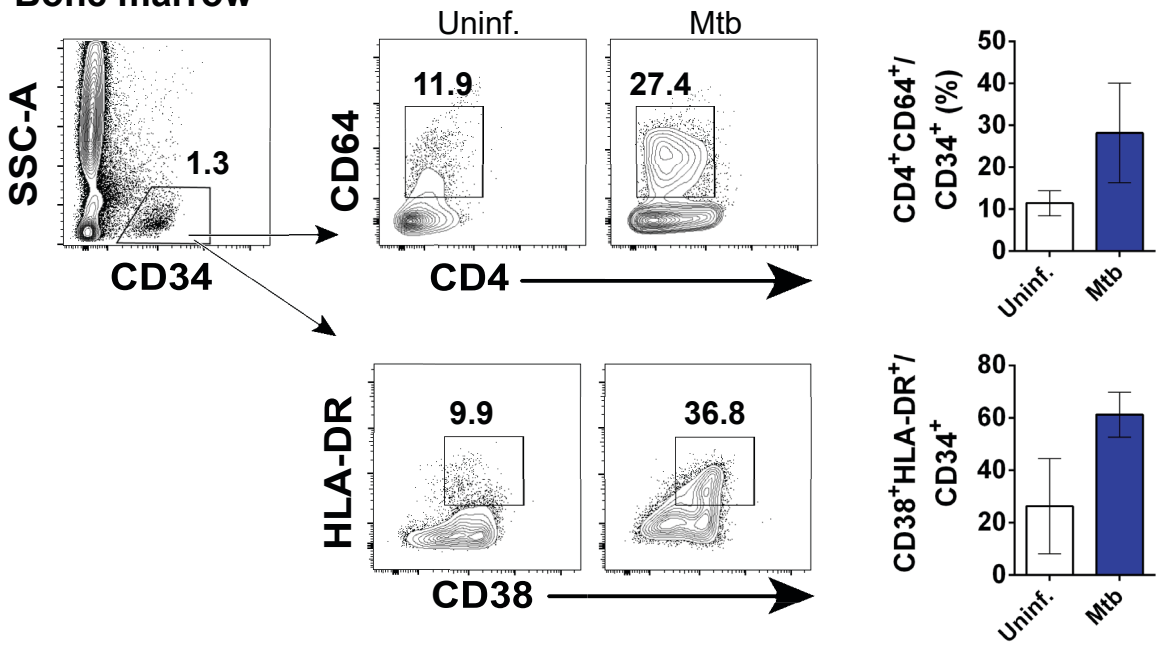

c

Peripheral blood

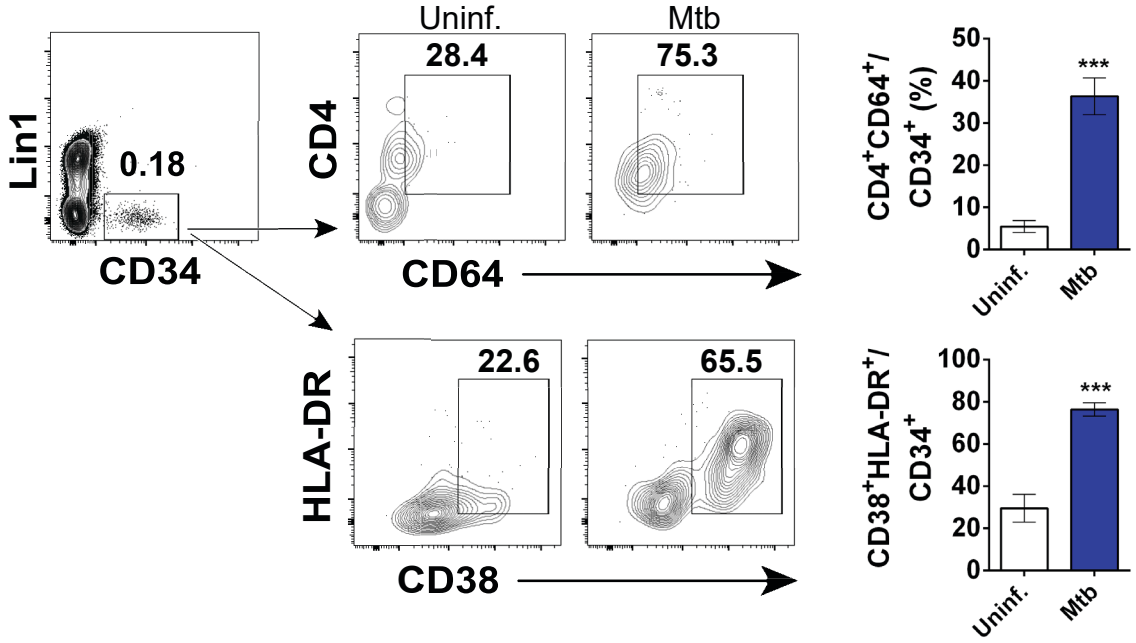

bioRxiv preprint doi: https://doi.org/10.1101/514943; this version posted January 9, 2019. The copyright holder for this preprint (which was not certified by peer review) is the author/funder, who has granted bioRxiv a license to display the preprint in perpetuity. It is made available under aCC-BY-ND 4.0 International license.

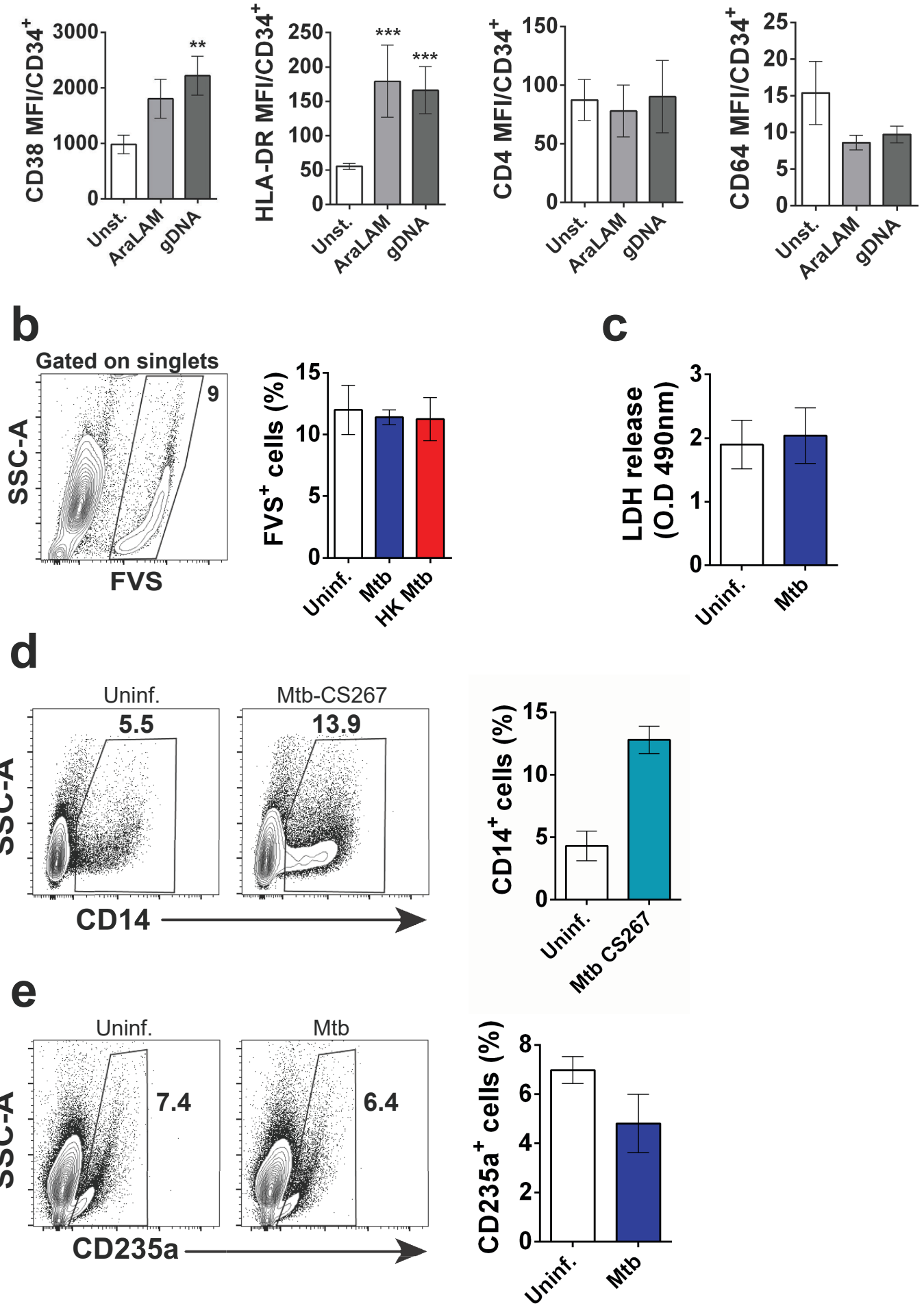

bioRxiv preprint doi: https://doi.org/10.1101/514943; this version posted January 9, 2019. The copyright holder for this preprint (which was not certified by peer review) is the author/funder, who has granted bioRxiv a license to display the preprint in perpetuity. It is made available under aCC-BY-ND 4.0 International license.

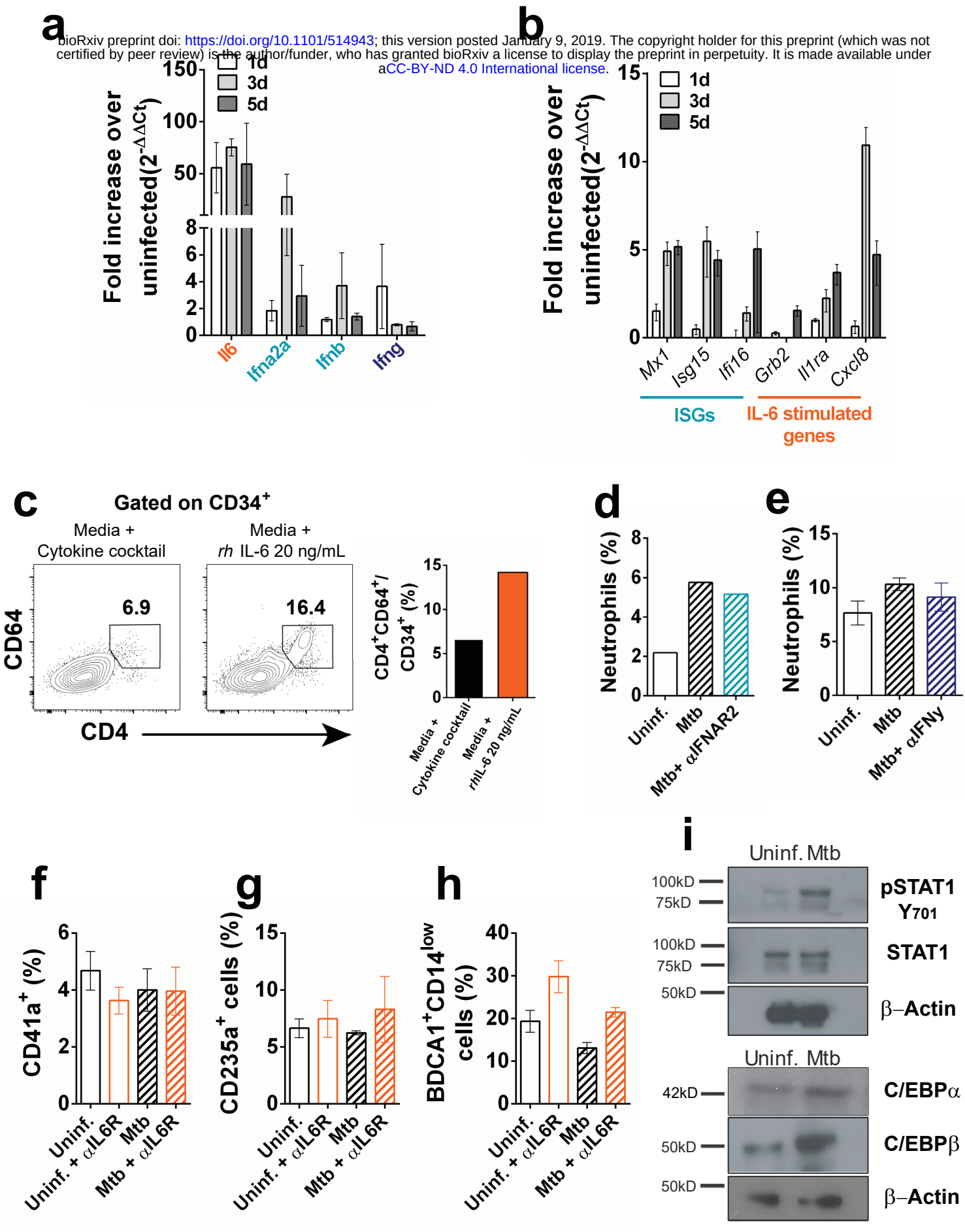
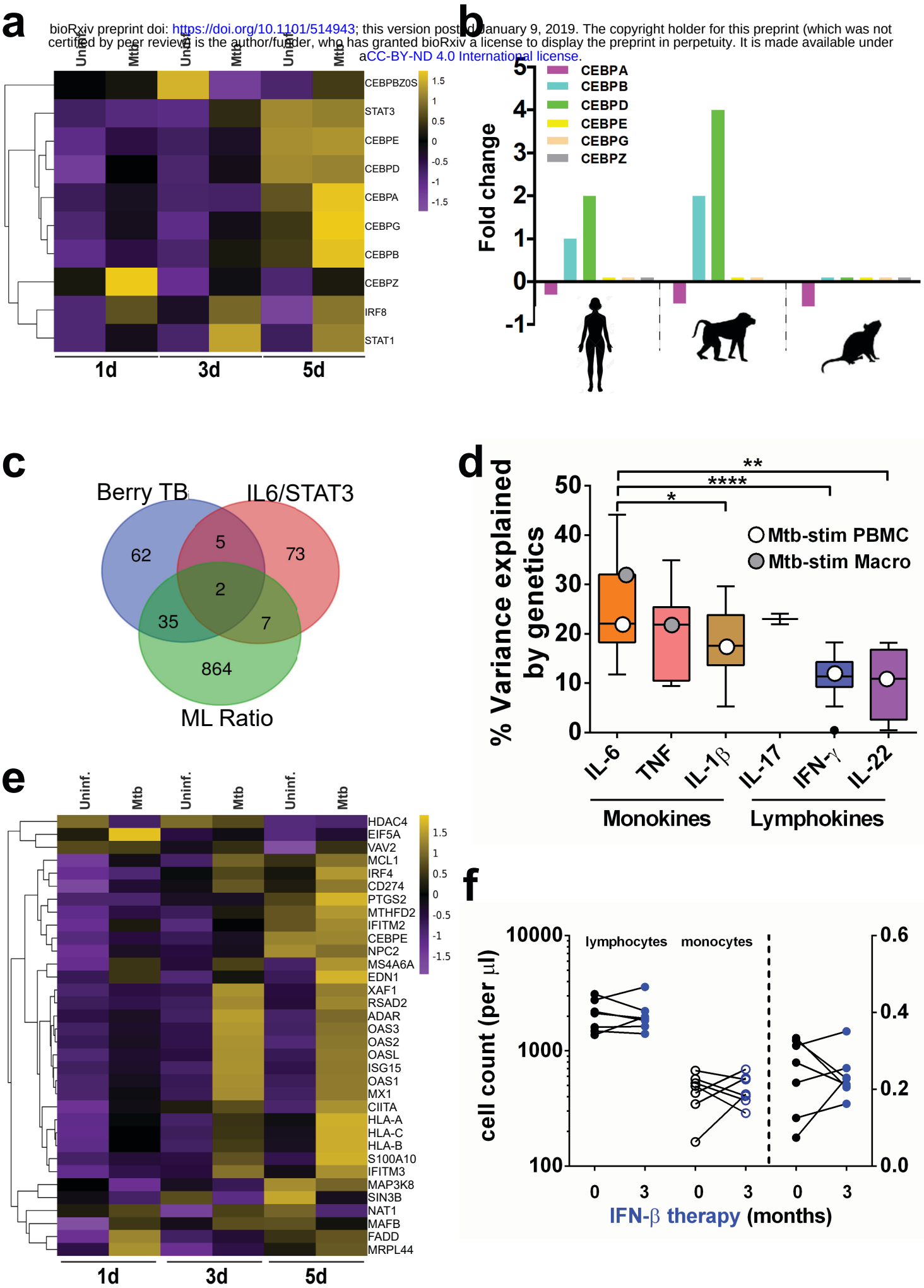
bioRxiv preprint doi: https://doi.org/10.1101/514943; this version posted January 9, 2019. The copyright holder for this preprint (which was not certified by peer review) is the author/funder, who has granted bioRxiv a license to display the preprint in perpetuity. It is made available under aCC-BY-ND 4.0 International license.